UNIVERSITY OF THESSALY
SCHOOL OF ENGINEERING
DEPARTMENT OF MECHANICAL ENGINEERING

Failure mechanisms in heat exchangers

by

Moschogianni Eleni

Supervisor
Prof. Gregory N. Haidemenopoulos

Submitted in partial fulfillment of the requirements for the degree of Diploma in Mechanical Engineering at the University of Thessaly
Volos, 2023

FAILURE MECHANISMS IN HEAT EXCHANGERS

Moschogianni Eleni

Department of Mechanical Engineering, University of Thessaly

Supervisor: Dr. Gregory N. Haidemenopoulos
Director, Laboratory of Materials

ABSTRACT

Heat exchangers are used for the transfer of heat from one process stream to another (combustion gases, hydrocarbon mixtures, steam, water, gases, liquids). They constitute critical pieces of equipment in many industrial processes. Failure of heat exchangers may cause financial damage but may also play an important role in process safety. The thesis aims to investigate the major mechanisms of failures in heat exchangers, such as corrosion, hydrogen damage, and mechanical failures. In addition, causes of failure will be investigated, such as imperfections during primary manufacturing of shell and tubes and activities during secondary manufacturing, such as tube straightening/bending, or cleaning. Design issues will also be discussed. Several case studies, from the literature as well as the research on failure investigations of the Laboratory of Materials (LoM), will be reviewed and characteristics will be highlighted. The thesis will provide an overview of the advances in the research area of failures in heat exchangers, and an empirical guide for the design of heat exchangers, the manufacturing routes, and the inspection and maintenance programs to minimize the risk and the negative consequences of heat exchanger failures.

Keywords: heat exchangers, mechanisms of failure, causes of failure, design issues, inspection, guidelines

ΜΗΧΑΝΙΣΜΟΙ ΑΣΤΟΧΙΑΣ ΣΕ ΕΝΑΛΛΑΚΤΕΣ ΘΕΡΜΟΤΗΤΑΣ

Μοσχογιάννη Ελένη

Τμήμα Μηχανολόγων Μηχανικών Πανεπιστημίου Θεσσαλίας

Επιβλέπων: Δρ. Γρηγόριος Ν. Χαϊδεμενόπουλος
Εργαστήριο Υλικών

ΠΕΡΙΛΗΨΗ

Οι εναλλάκτες θερμότητας χρησιμοποιούνται για τη μεταφορά θερμότητας από ένα ρεύμα διεργασίας σε ένα άλλο (αέρια καύσης, μείγματα υδρογονανθράκων, ατμός, νερό, αέρια, υγρά). Αποτελούν κρίσιμα κομμάτια εξοπλισμού σε πολλές βιομηχανικές διεργασίες. Η αστοχία ενός εναλλάκτη θερμότητας μπορεί να προκαλέσει οικονομική ζημιά, ενώ ταυτόχρονα διαδραματίζει σημαντικό ρόλο στην ασφάλεια της διαδικασίας. Η διατριβή στοχεύει στη διερεύνηση των κύριων μηχανισμών αστοχίας σε εναλλάκτες θερμότητας, όπως διάβρωση, βλάβες υδρογόνου και μηχανικές αστοχίες. Επιπλέον, θα διερευνηθούν τα αίτια της αστοχίας, όπως οι ατέλειες κατά την πρωτογενή κατασκευή κελύφους και σωλήνων, καθώς και δραστηριότητες κατά τη δευτερογενή κατασκευή, όπως το ίσιωμα/κάμψη σωλήνων ή ο καθαρισμός. Θα συζητηθούν επίσης θέματα σχεδιασμού. Αρκετές περιπτωσιολογικές μελέτες, από τη βιβλιογραφία καθώς και την έρευνα για τις έρευνες αστοχίας του Εργαστηρίου Υλικών (LoM), θα ανασκοπηθούν και θα επισημανθούν τα χαρακτηριστικά. Η διατριβή θα παρέχει μια επισκόπηση της προόδου στον ερευνητικό τομέα των αστοχιών σε εναλλάκτες θερμότητας και έναν εμπειρικό οδηγό για το σχεδιασμό των εναλλακτών θερμότητας, τις διαδρομές κατασκευής και τα προγράμματα επιθεώρησης και συντήρησης για την ελαχιστοποίηση του κινδύνου και των αρνητικών συνεπειών της θερμότητας αστοχίες εναλλάκτη.

Λέξεις κλειδιά: εναλλάκτες θερμότητας, μηχανισμοί αστοχίας, αιτίες αστοχίας, θέματα σχεδιασμού, επιθεώρηση, εμπειρικός οδηγός

CONTENTS

LIST OF TABLES

LIST OF FIGURES

1. INTRODUCTION

1.1 Motivation and Background

In many industrial processes, heat exchangers are essential, allowing an efficient thermal energy transfer from one medium to another. They are widely used in industries that involve power generation, oil and gas, and heating, ventilation, and air conditioning systems. The most common designs of heat exchangers that can be found are shell and tube heat exchangers, air-cooled heat exchangers, plate-type heat exchangers, spiral heat exchangers, and double-pipe heat exchangers, with each of these types being utilized for different applications, meeting specific standards [1]. Since they are operating for a long period, internal and external factors can affect their performance and efficiency [2]. To avoid catastrophic results and failures, it is necessary to examine not only the modes of mechanism that led to this but also the root causes that contributed to the failure mechanism. Failure mechanisms can be manifested in many ways, which can be categorized into four main types: mechanical, chemically induced corrosion, a combination of mechanical and chemically induced corrosion, and fouling. The first one involves metal erosion, steam or water hammer, vibration, thermal fatigue, freeze-up, loss of cooling water, and thermal expansion. The second type of failure mechanism comes in seven different varieties: general corrosion, dealloying, pitting corrosion, stress corrosion, galvanic corrosion, crevice corrosion, and condensate grooving. As a combination of mechanical and chemically induced corrosion, we identify erosion-corrosion and corrosion-fatigue. Finally, fouling involves precipitate

fouling- scaling, chemically-based fouling, and biofouling. The above mechanisms result in reduced heat transfer efficiency, structural fails, leaks, and pressure drops, affecting both the safety and the economy of the industry itself. To ensure reliability and efficiency the detection and mitigation of these modes of failure are necessary from the very early stages. Since maintenance and repair create a costly downtime period measures to enhance the longevity and performance of heat exchangers involve preventive measures, design modifications, material selection as well as inspection and maintenance programs [3]. The importance of heat exchangers to industrial processes creates a need to improve them by avoiding and resolving potential reasons that lead to their failure. This thesis aims to investigate the types of failure mechanisms and their root causes. The presentation of heat exchanger failure case studies will provide design guidelines for situations that differ in material selection, the external environment, the failed part, the design specifications, or the impact of human factor. The thesis will provide an overview of the advances in the research area of failures in heat exchangers, and an empirical guide for the design of heat exchangers, the manufacturing routes, and the inspection and maintenance programs to minimize the risk and the negative consequences of heat exchanger failures.

1.2 Historical review

Heat exchangers have been a crucial part of the equipment in industries, with the first ones dating back centuries, to the Roman and Chinese Empires. The heat exchangers, as we know them today started appearing in the late 18^{th} and 19^{th} centuries when engineers began developing and gradually improving them. An important invention requiring heat transfer to generate power was the steam engine, invented by James Watt. The first heat exchanger devices that have been reported were ‘pipe coil’ or ‘hairpin’ type. A revolution in the department of heat transfer technology was the invention of shell and tube heat exchangers in the mid-19^{th} century by French engineer Ferdinand Carre, a component that improved the efficiency of the existing ones and provided an increased heat transfer surface area. However, major advancements didn’t occur until the 20^{th} century, when efficient energy utilization became a need for every industry. That was the moment when plate and frame heat exchangers appeared with ever higher heat transfer rates and improved designs. Further research introduced finned tube exchangers and heat exchangers corresponding to specific applications.

Failures were always a problem that intrigued scientists to discover the failure mechanisms and how each of them evolved with the combination of the material, the external

environment, and the operational processes. Since the first heat exchangers were manufactured using iron and copper, materials prone to corrosion with corrosive fluids, corrosion was an important problem that led to the replacement of these materials by more resistant ones, such as titanium, stainless steel, and multiple other alloys.

Failure analysis is a scientific field that has been involved through the years to avoid and control failure mechanisms in heat exchangers. The aspects that researchers work on are material selection, prevention, monitoring techniques, and proper maintenance. Studies over the years have managed to identify material properties, operating conditions, and fluid composition with catastrophic effects on heat exchanger components. By extension to address the issues that have been mentioned above, further research has been conducted to identify conditions that will eventually improve heat exchangers efficiency. Those techniques involved surface treatments, enhancing the corrosion resistance of the materials, or advanced coating among others.

To sum up, the understanding of failure mechanisms in heat exchangers is a never-ending effort. Significant steps in the evolution of heat exchangers have been observed over the years to improve their reliability and efficiency. The findings of these studies provide useful guidelines and maintenance techniques to ensure the proper working of each type of heat exchanger.

1.3 Scope of this study

The key objectives of this thesis are presented below:

i. To identify and categorize the common modes of failure mechanisms
ii. To investigate the root causes that initially led to these failure mechanisms.
iii. To analyze the types of inspection to identify these failure mechanisms.
iv. To assess the impacts on safety and economy as a result of these failure mechanisms.
v. To provide an overview of case studies where these mechanisms are present.
vi. To propose recommendations and design guidelines to protect heat exchangers.

By attaining these objectives an improvement in the reliability, performance, and operational efficiency of heat exchangers can be achieved through the creation of practices that will minimize failure modes.

2. THEORETICAL BACKGROUND

2.1 Types of heat exchangers

A general function of a heat exchanger is to transfer heat from one medium to another. They are widely used in space heating, refrigeration, air conditioning, power stations, chemical plants, petrochemical plants, petroleum refineries, natural gas processing, and sewage treatment. An internal combustion engine represents the typical example of a heat exchanger in which a circulating fluid known as engine coolant flows through radiator coils and air flows past the coils. It reduces the temperature of the coolant and heats the incoming air. Another example is the heat sink- used in computers and many electronics. Heat sinks are passive heat exchangers that transfer the heat generated by an electronic or mechanical device to a fluid medium, often air or a liquid coolant.

The most commonly used types of heat exchangers are:

a. Shell and Tube heat exchangers,
b. Air-cooled heat exchangers,
c. Plate type heat exchangers,
d. Spiral heat exchangers and
e. Double pipe heat exchangers.

Shell and Tube heat exchanger: This type of heat exchanger is a class of heat exchanger designs. One fluid runs through the tubes, and another fluid flows over the tubes (through the shell) to transfer heat between the two fluids.

Air-cooled heat exchangers: Air-cooled heat exchangers also known as Fin Fan heat exchangers are typically used in applications where water is now available or the desired process outlet temperature can be achieved given the maximum ambient temperatures. Air-cooled heat exchangers are used in a wide variety of applications.

Plate-type heat exchangers: This particular heat exchanger is a type of heat exchanger where metal plates are used to transfer heat between two streams. This has a significant benefit over a conventional heat exchanger in that the fluids are exposed to a significantly bigger surface area because the fluids are spread out over the plates.

Spiral heat exchangers: It is made by rolling two long metal plates around a central core to create two concentric spiral flow passages, one of each fluid. There is no flow bypassing or intermixing since the plate edges are welded.

Double pipe heat exchangers: The double pipe heat exchanger, also known as a concentric pipe, hairpin, jacked pipe, and jacketed U-tube heat exchanger, consists of a single tube mounted inside another. One fluid flows in the inner pipe, while a second fluid in the outer pipe annuals.

Regarding *flow arrangement*, there are two main categorizations of heat exchangers: counterflow heat exchangers and parallel-flow heat exchangers. The fluids enter counter-flow heat exchangers from the opposing ends. The counter-current design is superior in terms of efficiency since it can transmit the most heat from the heat (transfer) medium.

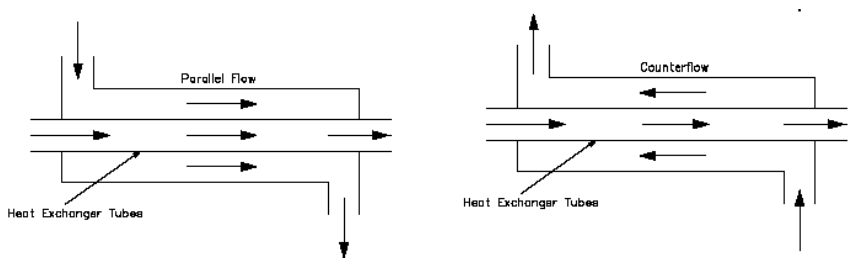

Figure 2-1: The two types of flow arrangement [1].

Heat exchangers are made with a minimum resistance to fluid flow through the exchanger and a maximum surface area between the two fluids for efficiency. Including fins or corrugations in one or both directions, which increase surface area and may channel fluid flow or create turbulence, can also impact the exchanger's performance.

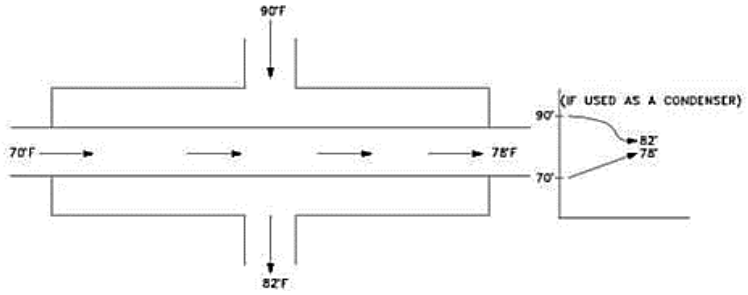

Figure 2-2: Temperature distribution across the heat exchanger [1].

The fluids in a cross-flow heat exchanger move almost perpendicular to one another.

The driving temperature across the heat transfer surface varies with position, but an appropriate mean temperature can be defined. In most simple systems this is the “log mean temperature difference” (LMTD). Sometimes direct knowledge of the LMTD is not available and the NTU (Number of Transfer Units) method is used. (which will be briefly described below).

2.2 Heat exchanger design basics

All heat exchangers must fulfill some basics such as the heat transfer theories, with the main equation referring to the heat transferred per unit of time:

$$Q = U \times A \times \Delta T_m$$

Where Q has units (W), U stands for the overall heat transfer coefficient with units (W/m^2. °C), A stands for the heat transfer area with units (m^2) and ΔT_m stands for the mean temperature difference, the temperature driving force (°C).

For heat transfer exchangers two types of calculations may need to be done. For a new heat exchanger design, the heat duty and the temperature difference are usually known meaning that the hot and cold fluids have been specified, along with the flow rate and temperatures. For this case, the goal is to determine the heat transfer coefficient U, and the size of the heat exchanger, A.

The size is given for an existing heat exchanger, so the overall heat transfer coefficient needs to be re-estimated. This happens because there may be a significant amount of falling and it needs to be determined whether the extent of falling is acceptable or not or whether the heat exchanger needs to be cleaned.

The design of an exchanger is an iterative procedure since the heat transfer coefficient and pressure drop depend on many geometric factors that are part of the design process. These factors for example for a shell and tube exchanger include diameters, tube length and layout, baffle type and spacing, and the number of tube and shell passes. All of these design parameters affect the heat transfer area as well as the heat transfer coefficient by affecting the flow properties of the fluid thus it becomes an iterative procedure.

Typically, some conditions like inlet conditions are given, such as temperatures, pressures, compositions, flow rates, and phase conditions of the two inlet streams. That defines the ΔT as well as the heat duty. If a heating or cooling utility is to be selected, it is selected from a standard table along with its inlet and exit temperatures. For example, if ambient air or water from natural sources is being used then the inlet temperature is defined and the exit temperature will probably be restricted by environmental regulations.

The design commences with the allocation of the streams based on the properties and conditions of the two streams. With this information being established, an overall energy balance is carried out to calculate the streams' heat duty and the remaining exiting conditions.

Also, if a utility stream is used, its flow rate is calculated from an overall energy balance.

$$m_H \times Cp_H \times (Ti_H - To_H) = m_C \times Cp_C \times (To_C - Ti_C)$$

Where m_H stands for the mass flow rate of the hot fluid in kg/hr., Cp_H for the mass heat capacity of the hot fluid in Joules/kg^{0}C, $Ti_{H,}$ and To_C stand for the inlet and outlet temperatures on the exchanger cold side in ^{0}C, m_C for the mass flow rate of the cold fluid in kg/hr., Cp_C for the mass heat capacity of the cold fluid in Joules/kg^{0}C and *TiC* and *ToC* stand for the inlet and outlet temperatures on the exchanger's cold side in ^{0}C.

The next step is checking the temperature crossover. Assuming a 1-1 exchanger with countercurrent flow, a check is made so that the *second law of thermodynamics* is not violated and a reasonable ΔT exists at the end of the exchanger. If a phase change occurs on either side of the exchanger a heating or cooling curve is calculated to check for any temperature crossover.

During the initiation process, an overall heat coefficient is assumed from the standard range of values for the given system and the estimated area can be calculated. If it is too large (>8000 ft^2), multiple heat exchangers with the same area can be used in parallel.
Lastly, in most cases, a correction factor F_t needs to be calculated with a desired price of $Ft>0.85$ to define the configuration of the heat exchanger (number of shell and tube passes).

2.3 Common Modes of Failure

2.3.1 Mechanical

These failures may manifest in one of the following seven ways: metal erosion, steam or water hammer, vibration, thermal fatigue, freeze-up, loss of cooling water, and thermal expansion.

Erosion

In general, corrosion is an electrochemical reaction between a metal and its environment. Erosion is caused by flow restriction or a change of direction. It is increased if the flow contains solid particles or bubbles in liquids and by the two-phase flow. When corrosion is present erosion tends to accelerate the phenomenon.

It has been found that the majority of failures of tube heat exchangers are due to solid particle erosion [3]. Most metal erosion problems that lead to metal loss take place at the tube inlets and the inside wall of the tubes especially when the containing fluid consists of solid particles. The most critical regions involve the U-bend of tubes and the tube entrances [1]. However, erosion issues can also be seen on the outside of tubes, typically as a result of wet, fast-moving gases like steam impinging on them [3].

The wear of the heat exchangers depends mainly on the velocity of solid particles. Both high and low velocities lead to catastrophic results with the first destroying the surface protective film and the last resulting in heavy deposition upon the tube surface. An empirical expression that can be used to determine the relationship between erosion and velocity is Erosion $\propto$ Velocity^{n,} where n depends on material selection and operating conditions with values from 2.3 to 2.7 for ductile materials and 2 to 4 for brittle materials [5]. The effect of flow velocity and particle size can also be calculated using the Lagrangian tracking method. The results define that erosion cannot be avoided while solid particles are present inside the fluid [4]. Another important factor is the impact angle φ between the two-phase stream and the surface. The maximum wear of ductile materials occurs in low impact angles for φ max = 20^{o}–40^{o} whereas less severe erosion is observed between 10^{o}-30^{o}. Brittle materials occur for perpendicular impact and increase with the increase of the angle of impingement.

Additional factors resulting in material degradation due to erosion are the particle shape and diameter, the particulate concentration, and the hardness of the erodent. Concerning the shape of the particle it has been proven that angular particles are more susceptible to erosion than spherical while shape determines other important factors such as the angle and the velocity which have been analyzed above. The particle's diameter influences the erosion rate at the range of 50-100 μm. Above that range, it does not affect in any way the erosion rate. As particulate concentration rises, erosion rises linearly up to a point before decreasing due to particle-particle interactions [5,6].

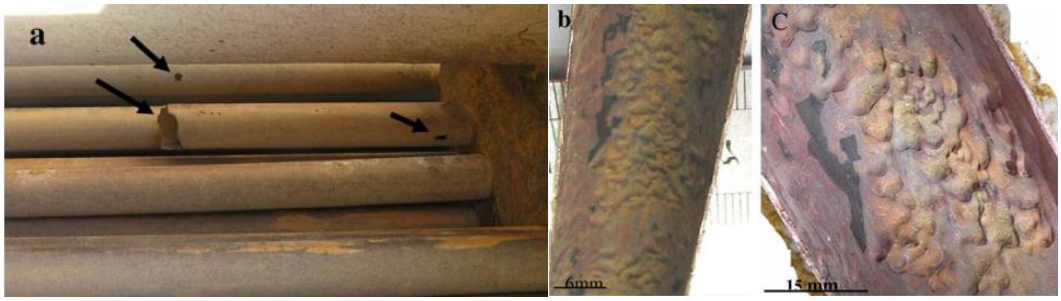

Figure 2-3: Flow-induced erosion due to a change in the velocity of circulating water. (a) Flow-induced erosion inside tube surface. Arrows indicating the locations where tube thickness is reduced and finally got holed, (b) horse-shoe appearance, and (c) the same effect at higher magnification [2].

Steam or Water, Hammer

A sudden change in fluid velocity results in a pressure or momentum transient, commonly referred to as a steam hammer or water hammer, in a closed system. It is categorized based on what caused the velocity shift [9]. Responsible for the rupture caused by the water

hammer might be factors such as the presence of slugs, high-pressure surge, blockage at the tube entrance and tubes, the volumetric difference between the steam and the water, presence of condensed water droplets, increased inlet flow and decreased inlet water temperature [10]. The prices that have been measured for pressure surges that can result in rupture or collapse have to exceed 20,000 psi. In a horizontal pipe heat exchanger, the slugging starts the water hammer. The flow pattern abruptly alters when slugs are present. The onset of water hammer in heat exchangers is highlighted by the transition slug flow and large-scale slug flow pattern. As a result, when a barrier is reached, the steam or liquid's kinetic energy transforms into pressure energy. Attention must be given to flow control valves to prevent hydraulic shock from sudden moves [9,10].

Vibration

We can determine the vibration failure mechanism as a mechanical phenomenon that creates oscillations in the material at an equilibrium point [11]. Flow-induced vibrations seem to be a problem in designing heat exchangers. U-bend regions tend to experience this problem, where the tube natural frequencies are usually low or in areas where localized high velocities are produced, such as baffle plates, entrance, and exit nozzles, baffle plates, or open tube lanes [12]. The mechanical integrity of a heat exchanger can be found based on some excitation mechanisms, which are the following:

i. fluidelastic instability;
ii. vortex shedding;
iii. multi-phase buffeting;
iv. acoustic resonance;
v. turbulence buffeting;
vi. hydraulic transients;
vii. environmental excitation;
viii. transmitted mechanical vibration.

The first one is the most severe type of mechanism and can cause damage in a very short period of operation. The wake moving in response to the tube displacement generates forces on the tube. As the tube moves the flow redistributes and the force on the tube associated with the redistribution enhances the tube motion [13]. Instability occurs when the energy absorbed by fluid forces exceeds the energy released by damping during a single vibration cycle [14]. Different approaches concerning this particular mechanism have been given by

different scientists, providing the scientific community with some basic design guidelines [12].

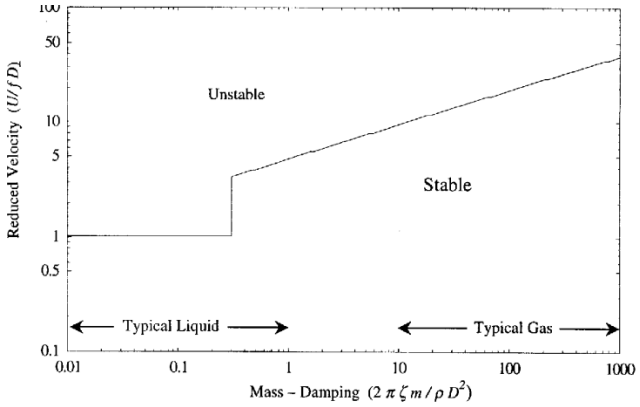

Figure 2-4: Fluidelastic stability chart for a rotated triangular geometry [13].

The following assessment equation emerges:

$$\zeta > \frac{D^2}{16\pi\text{^}2} \int_0^L \left(\frac{U(x)}{fD}\right)^2 \rho(x) C(x) \varphi\text{^}2(x) dx$$

Where ζ stands for the actual damping ratio for the tube and x for the distance along the tube which is of total length L. Most of the key parameters are allowed to vary along the length of the tube to model the varying flow conditions at different points in the heat exchanger, thus the density, ρ(x), the gap flow velocity, U(x), the tube energy, φ^2 (x), and a lift coefficient, C(x), are all functions of location x. For a standard assessment, it is convenient to determine the damping required to prevent fluidelastic instability using the above equation and then compare this value to values measured for actual heat exchangers in Figure below.

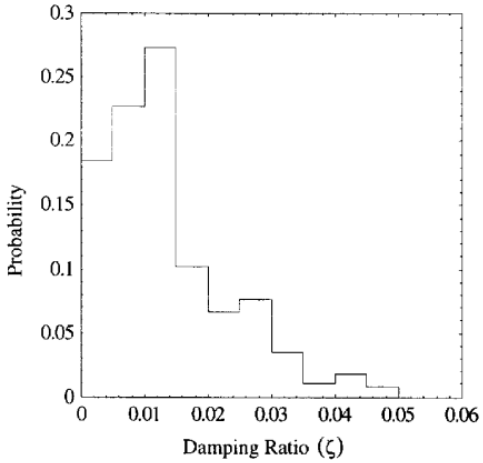

Figure 2-5: Experimental values for the damping ratio of heat exchanger tubes [13].

In vortex shedding, every wake behind every tube oscillates. An oscillating force acts on the tube due to the wake's oscillation frequency, which is inversely proportional to the flow

velocity. The oscillating force is in a direction that is opposed to both the flow and the tube's axis. The wake oscillation is connected to the vorticity being shed from the stationary area in the wake behind a tube. This vorticity alternately exits the tube from one side and then the other, creating an oscillating effect. The conditions for lock-on are usually estimated from:

$$0.8f < f\mathrm{v} < 1.2f \quad with \quad fv = St\frac{U}{D}$$

where f is the tube natural frequency and f is the frequency of vortex shedding. The frequency of vortex shedding is given by the second equation in which St is the Strouhal number. Vortex-induced tube vibration can often not be avoided in gases, however, damping in gas flows is generally sufficient to prevent large amplitudes of vibration. Vortex-induced vibration is, thus, of most concern in liquid flows or gas flows where tubes have very small damping [13].

Thermal fatigue

Thermal fatigue occurs as a result of temperature differences across the tube or due to imposed system operations. This type of failing mechanism seems to appear particularly in the U-bend area [3,7] with the highest equivalent thermal stresses being observed at the joints of tubes and tube sheets.

Fatigue is a result of repetitive thermal cycling associated with accumulated thermal stresses [15]. It needs to be emphasized that thermal stresses are as important in corrosion fatigue as mechanical stresses [7].

The results of thermal fatigue usually appear in the form of cracking where at the beginning it's hard to see but eventually turns out disastrous and completely severs the material. We can assume that when stresses exceed the fatigue limit the failure begins initially with the growth of circumferential crack about the tube periphery [16].

Stresses can be calculated using the Von Mises criteria equations to determine the equivalent structural and thermal stress equivalents.

$$\Delta\sigma = (\sigma_{11} - \sigma_{11}^{LT})_m - (\sigma_{11} - \sigma_{11}^{LT})_n$$

$$(\Delta S_{p,k} - \Delta S_{LT,k}) = \frac{1}{\sqrt{2}}[(\Delta\sigma_{11} - \Delta\sigma_{22})^2 + (\Delta\sigma_{11} - \Delta\sigma_{33})^2 + (\Delta\sigma_{22} - \Delta\sigma_{33})^2 + 6(\Delta\sigma^2_{12} - \Delta\sigma^2_{13} + \Delta\sigma^2_{23})0.5]$$

Similarly, we can obtain the local heat equivalent stresses:

$$\Delta\sigma_1^{LT} = \sigma_1^{mLT} - \sigma_1^{nLT}$$

$$\Delta S_{LT,k} = \frac{1}{\sqrt{2}}[(\Delta\sigma_1^{LT} - \Delta\sigma_2^{LT})^2 + (\Delta\sigma_1^{LT} - \Delta\sigma_3^{LT})^2 + (\Delta\sigma_2^{LT} - \Delta\sigma_3^{LT})^2]^{0.5}$$

Where $\Delta S_{LT,k}$ stands for the local thermal equivalent stress, $\Delta S_{p,k}$ is the reduction in fatigue strength.

The alternating stress in the system is given by:

$$S_{alt,k} = (k_f * k_{e,k} * (\Delta S_{p,k} - \Delta S_{LT,k}) + k_{v.k} * \Delta S_{LT,K})/2$$

Where if stands for the fatigue strength reduction factor, $k_{e,k}$ is the fatigue penalty factor, and $k_{v,k}$ is the Poisson correction factor (usually assumed to be 0.3).

With the above calculation, the permissible number of cycles and fatigue damage can be found taking into consideration the properties of the material and the range of stresses at a specific temperature [15].

Thermal fatigue can be accelerated by insufficient cooling (potentially caused by water leakage) or the existence of an oxide layer which can cause an important rise in temperature [17].

Freeze-up

This type of failure mechanism refers to cases where the temperature falls below the freezing point of either fluid in the heat exchanger. The abrupt release of refrigerant pressure from the condenser also contributes to this sort of failure. The pressure abruptly drops below the refrigerant's boiling point as a result of a line break or relief valve discharge. Water in the tubes freezes when it is heated through boiling. Freeze-up is mostly common in evaporators, condensers [3], and borehole heat exchangers. The last often presents freezing problems due to their need to operate in some cases below the water freezing point. In addition, the freezing-induced ice pressure can damage the grout. It has been determined that grout failure due to freezing is significantly influenced by porosity and permeability [18].

Loss of cooling water

Before a flow of hot gas is initiated, compressed air aftercoolers and gas coolers should always have a supply of cooling liquid. high-temperature gas. If there is not enough cooling liquid, the tubing may melt or deform. The following figure refers to the case where the cooling fluid was not enough resulting in the deformation of the presenting tube [3].

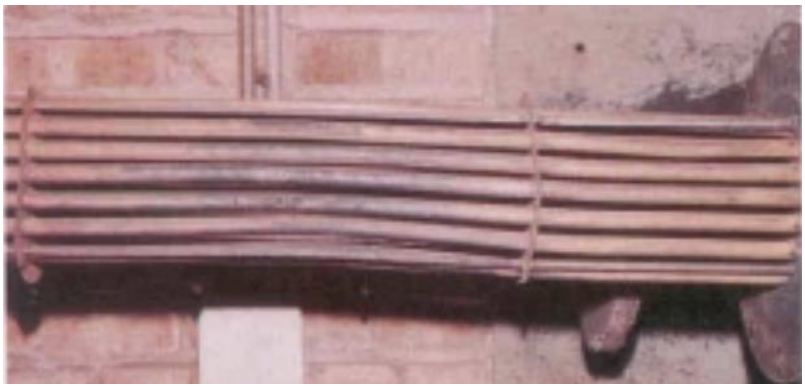

Figure 2-6: Tube Warping because of insufficient cooling water [3].

Thermal expansion

The tendency of matter to alter shape, volume, and area in reaction to a change in temperature is known as thermal expansion. Temperature has a monotonic relationship with a material's average molecular kinetic energy [19]. In our case, continuous heating leads to high pressures that heat exchanger components cannot bear. This failure mechanism is typical in steam-heated exchangers but it can also appear in any form of hot fluid that is valved off without thermal expansion protection [3]. Thermal expansion affects immediately other failure mechanisms such as corrosion fatigue since mechanical loads and stresses in heat exchanger components are reinforced by it [10]. In many cases, startup problems have been connected with thermal expansion because of temperature differences [16].

Finally, it’s important to point out the material choice since the issue is frequently exacerbated by the use of joint components made of materials with varying thermal coefficients of expansion, such as stainless-steel tube sheets [20].

2.3.2 Chemically induced corrosion

The intricate chemical reactions between the components of the heat exchanger and the fluids that are pumped through it cause these problems. Chemically induced corrosion failures come in seven different varieties: general corrosion, dealloying, pitting corrosion, stress corrosion, galvanic corrosion, crevice corrosion, and condensate grooving.

General corrosion

General corrosion can be described as the regular disintegration of the surface metal [21]. The results of this type of corrosion appear as a uniform attack over the tube, tube sheet, or shell [3]. General corrosion is not catastrophic as long as there is no significant change in the water's chemistry but the fact that in many cases evidence that it’s taking place is not easily visible, can cause severe damage [3,21].

Materials prone to general corrosion are made of carbon steel, leading to rusting, and copper alloys leading to wall thinning. Although copper usually provides a lifetime of 25 years, copper alloys deposited on tube walls result in premature failures due to liquid metal embrittlement [21]. Finally, aggressive conditions like low PH (less than 7) in combination with carbon dioxide or oxygen accelerate the attack on copper. In general, chemicals and acids are quite dangerous for metal loss [3].

This type of failure mechanism can be a result of deliberately designing a heat exchanger with a limited life, mistaken choice of materials, miscalculation of the corrosive effect of the medium circulating through the heat exchanger, and improper chemical cleaning. Regarding the material choice, the existence of acid itself might not be disastrous, but if there has not been paid attention to the dew point, the internal surfaces of tube walls are susceptible to corrosion [7].

Finally, aggressive conditions like low PH (less than 7) in combination with carbon dioxide or oxygen accelerate the attack on copper. In general, chemicals and acids are quite dangerous for metal loss.

Dealloying

Dealloying is a form of corrosion and occurs when one element of an alloy is removed through the corrosion process and the structure retains its appearance while becoming wicker structurally.

A common problem that mainly yellow brass (an alloy that contains 80% copper and 20% zinc) tubes suffer from and is related to dealloying, is dezincification. Alloys containing a percentage of more than 15% of zinc are prone to erosion. In addition, if the containing water is high in salts content, layers of depositions might be created with areas of differential aeration and concentration cells which promote plug formation. In this process, Zinc is selectively leached out from Cu-alloys and results in a porous and weak layer of copper and copper oxide. Dezincification eventually penetrates the metal, leading to further weakening and leakage of the structure [2].

Dealuminification is another possible failure mechanism for tubes manufactured from aluminum. Depending on the atmosphere and the amount of aluminum in the bronze, dealloying may occur. Through this mechanism, aluminum is selectively corroded, leaving behind porous copper that preserves the component's original dimensions and shape. The dealloyed material's mechanical properties, however, have drastically declined. This

mechanism is dependent on the aluminum content of the aluminum bronze, the cooling rate during fabrication, and the presence of a local crevice [8].

Pitting corrosion

A localized type of corrosion known as "pitting corrosion" can develop on passivated surfaces. Surface inclusions or grain boundaries may serve as the point where destruction begins. At some locations, aggressive anions penetrate the film and create small pits [22].

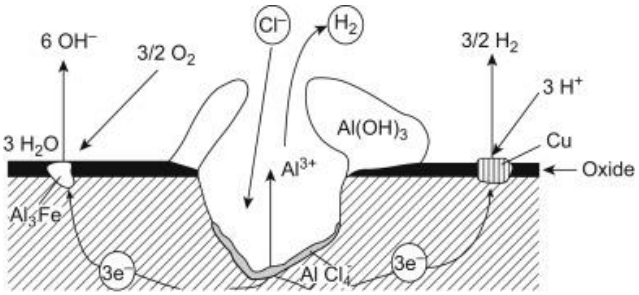

Figure 2-7: Mechanism of pitting corrosion of aluminum [23].

A pit, cavity, or small hole will emerge when an anodic reaction in a small area (exposed metal) sustains a cathodic reaction in a wide area (coating). Even in the absence of an oxygen supply, the metal oxidizes. When the small anode is subjected to a large cathode's high electron demand, severe pitting corrosion results. It will have very severe effects and be subtle while happening quickly. While corrosion is occurring deep within the metal structure below, only a little area of rust is visible on the surface [23].

Despite several studies and publications on the subject over the last century, pitting corrosion is a very complex process that has not yet been fully understood [22].

Pitting affects both ferrous and non-ferrous metals and has a direct connection with the presence of hydrogen and chloride.

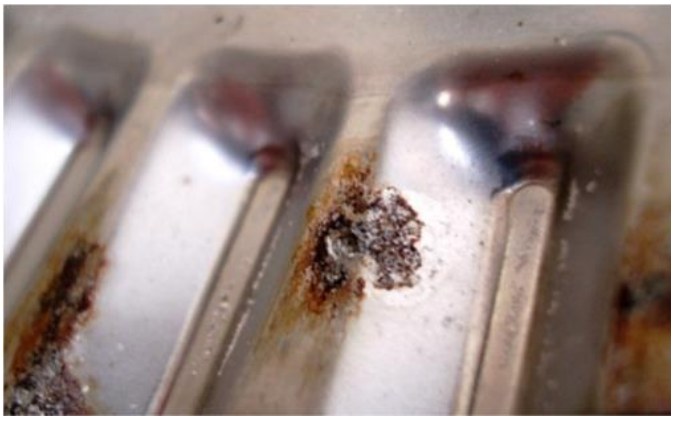

Figure 2-8: Pitting corrosion on the border area of failed heat exchanger plates [26].

The pits initiate on surface compositional heterogeneities or scratches. The susceptibility to pitting corrosion increases with the existence of dirt or scale deposits, scratches, breaks in metal surface films or breaks in protective scale layers, surface defects, and grain boundary conditions [3,25].

While hydrogen enters the heat exchanger the concentration of hydrogen atoms results in hydrogen embrittlement in the case of high-strength steel and enhances the susceptibility to pitting in the case of stainless steel. The presence of by-products such as NH3, HCl, and H2O generated by the reaction between nitride, chloride, oxygen impurities, and hydrogen in the feedstock is inevitable during hydrocracking. As a result, NH4Cl salt is produced. It is common for NH4Cl and NH4HS salts to be produced during the hydrocracking process, with NH4Cl beginning to precipitate above the dew point of vapor and NH4HS precipitating in the temperature range below the dew point. This indicates that it is more likely that NH4Cl salt will occur after the reactive effluent has been cooled. Failure analysis has proven that the presence of hydrogen weakens the stability of the protective film, while in the absence of hydrogen, there is less to no pitting corrosion. Another finding related to this was that chloride ions were more prone to replace OH^- rather than O^{2-}, another proof that indicates that oxygen increases the metal's susceptibility to pitting corrosion [24].

Stress corrosion

Season cracking, also known as stress-corrosion cracking (SCC), is the occurrence of susceptible alloys spontaneously cracking when certain corrosive conditions and sufficiently high tensile stresses are present at the same time [28]. That exact combination makes the stresses needed for the fracture to be less than the ones in case no corrosion is taking place [7]. This mechanism usually appears in the form of fine cracks attacking the grain boundaries in stress areas and can be observed easily on the surface of tubes and specifically on the inner surface [3,28].

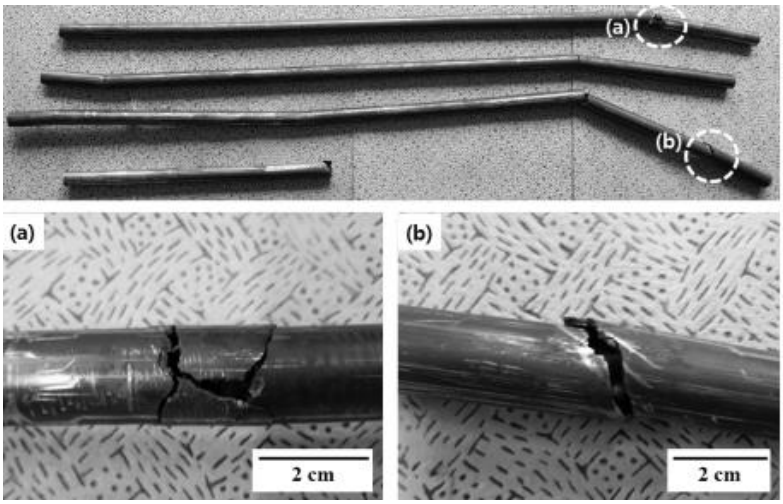

Figure 2-9: Photographs of the failed tubes; (a) circumferential and longitudinal direction crack, and (b) circumferential direction crack [32].

For SCC to occur the alloy must contain one of the many corrosive substances. Regarding copper and copper alloys an example of this corrosive substance in copper zinc alloys is ammonia [7]. One ppm or less of a concentration can be problematic. Ammonia-caused cracking usually appears in the inner U-bends of the heat exchanger tubes [3]. In addition to this, in copper alloys, the source of stresses might include residual stresses from non-uniform plastic strain during cold forming of alloys or normal service. In this case, cracking can be transgranular, intergranular, or mixed [7,28].

For brass alloys, the susceptibility to SCC is related to the amount of Zn on the alloy. Cracked regions, which often display noticeably branching transgranular fracture patterns, define the damaged look in aluminum brass tubes [28]. Carbon alloys are quite prone to SCC since the harmful environment seems theoretically normal. An example is the presence of sodium hydroxide or a wet hydrogen sulfide environment.

Finally, austenitic stainless steels fail when acid chlorides (a concentration of more than 500ppm leads to SCC [31]) and fluorides, and acid polythionic are induced. When they are in hot chloride and hot alkaline solutions SCC is a common mode of failure [28,29]. The chloride stress corrosion can become a threat when temperature and chloride concentration increase [3]. Special attention must be given when SCC is induced by polythionic acid (H2SnO6, where n = 2–5). During operation, the inner surface of the tubes changed into a sulfur-bearing scale due to the presence of H2S in the atmosphere. If there are still internal tensions present, this could encourage the production of polythionic acid in combination with vapor in the moist air of the atmosphere at the inner tube surface during downtime, which could lead to cracking [30].

Galvanic corrosion

Galvanic corrosion is one of the most common modes of corrosion involving a metal contacting another conductive material in a corrosive medium. It occurs in heat exchangers when two different metals mix in the presence of an electrolyte, such as acidic water. The relative potential of materials to withstand this kind of corrosion is displayed on the galvanic chart.

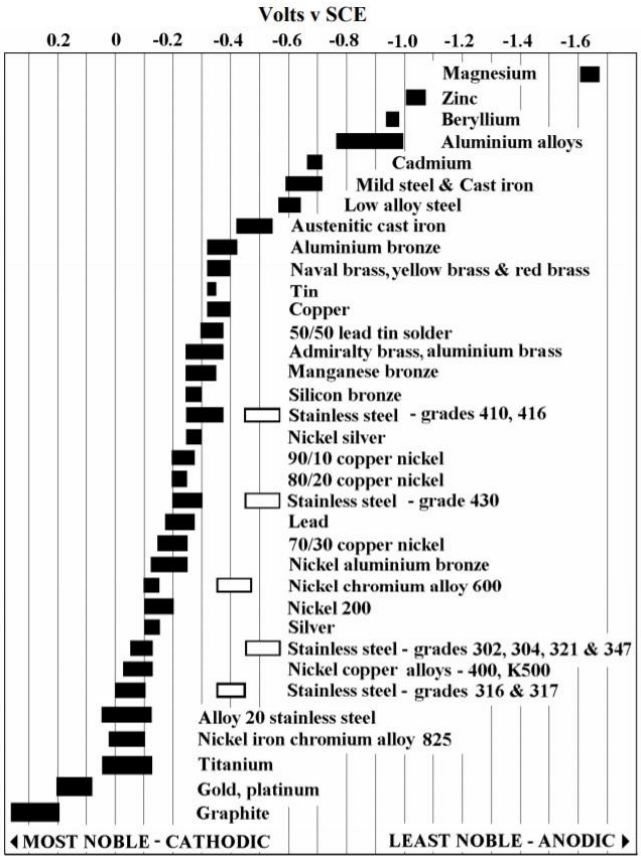

The series makes it possible to choose materials efficiently, allowing for the selection of metals with the lowest propensity to undergo a galvanic reaction.

When two metals from significantly different groups are combined in an electrolyte, significant corrosion of the less noble metal follows. Metals grouped have a relatively low ability to induce galvanic corrosion [3]. It has been found that the galvanic effect depends on the conductivity of the electrolyte [33].

Figure 2-10: Most noble to least-galvanic series.

Crevice corrosion

Crevice corrosion is defined as corrosion that takes place in confined regions of the metal surface where the environment has limited access [35]. Although this type of corrosion happens frequently it's not easy to identify and it's often been mistaken as erosion because of metal loss. New installations are susceptible to crevice corrosion since the protective film is not fully formed.

Regarding iron-based alloys hydrated ferric hydroxide is formed by the combination of water and ferrous hydroxide. The absence of oxygen results in products such as green hydrated magnetite or black anhydrous magnetite. A similar mechanism appears in copper alloys [3,7].

In heat exchangers, locations prone to crevice corrosion are gaps formed between tubes and tube sheets. These gaps might be a result of tube expansion due to inappropriate environments [34,35]. Another explanation for crevice appearance is the pressure of high-temperature hot water, which results in the creation of narrower crevices and compressive stress between crossing contact points at low-temperature hot water sides of corrugated plates. Numerous corrosive substances, including Cl, are gathered in a narrower crevice, and compressive stress causes fretting as the water pressure changes. Crevice corrosion occurs initially in crossing contact points where fretting has destroyed the surface passive coating [36].

Conditions that initiate this failure mechanism can be bubbles on the surfaces, cracks in the mill scale, inhomogeneity of the material, and local breakdown of protective film in addition to differences in concentration of oxygen or of soluble contaminants like chlorine. It's also often triggered by water containing dissolved solids [7].

It is a complex mechanism as it involves many stages.

In the first stage, a crevice is formed in and around secluded and hidden areas or under dirt or loose scale [3]. This creates a narrow space between the two metal surfaces where the diffusion of substances becomes hindered leading to the stagnation of corrosive substances. Due to naturally occurring reactions the oxygen quickly depletes in the gap and the concentration of metal ions increases. This leads to the formation of a galvanic couple with the crevice becoming anodic and the surrounding area becoming cathodic [34].

The cathodic reaction is the following:

$$\frac{1}{2}O2 + 2H20 + 2e^{-} \rightarrow 4OH^{-}$$

This reaction causes an oxygen concentration gradient inside and outside of the crevice as well as anodic dissolution inside the crevice, which can be described by the following reasons:

$$M \rightarrow M^{++} + 2e^{-}$$

The galvanic couple accelerates corrosion in the crevice in the second stage by reducing oxygen at the cathode. [34,35] The pH will consequently decrease as a result of the removal of OH- ions from the solution during the precipitation of these hydroxides, as demonstrated in the accompanying reaction [35].

$$M^{n+}(Cl^{-})2 + 2H20 \rightarrow M(OH)2 + 2H^{+} + Cl^{-}$$

Therefore, the anode's positive potential attracts negative hydroxide and chloride ions into the crevice. The hydroxide and chloride ions within the crevice react with the metal, gradually making the anodic region more acidic.

The third step takes place when the PH within the fissure falls to a critical level, forcing the passive layer to break down. At this point, corrosion progresses rapidly until the structure eventually fails [34].

Condensate grooving

The tubes of the steam-to-water heat exchanger have this issue on the outside, especially around the U-bend. As the condensate drains from the tubing in the form of rivulets, it can be identified by an irregular groove or channel cut in the tube. The electrical potential differential between the dry and wet portions causes a corrosion cell to typically develop in the wetted area [3]. Grooves can also occur from ammonia corrosion, leading to wall thinning. When the environment PH is around 8-9, ammonia destroys the protective layer and copper-based metals. The existence of ammonia can be justified as ammonia-contained compounds, such as (N_4H_6CO) and hydrazine N_2H_4 are used in feed water to remove dissolved oxygen. The following chemical processes can be used to describe how brass corrodes when ammonia is present.

$$Cu + 2NH3 \rightarrow Cu(NH3)2^{+} + e^{-}Zn + 4NH3 \rightarrow Zn(NH3)4^{2+} + 2e^{-}$$

Ammonia dissolves the copper oxides' passive layer (Cu_2O and CuO) forming complex compounds of cuproamines ($Cu(NH_3)_2$, $Cu(NH_3)_4$) and zincoamines ($Zn(NH_3)_4$). [37]

2.3.3. Combination of mechanical and chemically induced corrosion

In many cases, a heat exchanger failure results from a mixture of several conditions rather than one single reason. One or more locations might have simultaneous pitting corrosion, galvanic corrosion, and crevice corrosion attack, for instance. Quite often, a mechanical issue with a corrosion issue leads to a faster failure than either issue by itself. Two common types of combinations exist: erosion-corrosion and corrosion-fatigue.

Erosion-Corrosion

We determine erosion-corrosion (EC) as the combination of these two effects, accelerating one another, resulting in faster degradation of the material and higher levels of damage. Erosion-corrosion involves a series of simultaneous reactions developing a mechanistic model considering electrochemical reactions. Wall thickness defines EC wear with erosion disturbing the material's surface coating, because of high velocities, suspended solids, or

mechanical vibration, and corrosion removing the surface coating due to electrochemical processes like metal oxidation or dissolution. According to research by Brookhaven's National Laboratory, the localized distribution of flow, water chemistry, such as dissolved oxygen concentration, pH, and the corrosiveness of the flowing corrodent, high temperature and ambient pressure, and suspended particulates in the water are a few of the elements that affect EC wear. These elements typically interact to create EC wear [38]. Relative movement of the solids about the surface wears down a metal surface, especially when a fluid is forced to shift directions or when significant shear stresses are present [39].

Figure 2-11: Erosion-corrosion attack [39].

We detect this failure mechanism usually below the shell inlet nozzle, inside the U-bend area of tubes, particularly the tighter bends, in the entrance area of tubes, or at the point of contact with baffles and tubes [3]. When tubes contain fluids like inferior crude oil special attention must be given because of the nitrogen and sulfur compounds that crude oil contains. These compounds impose a high risk of failure [40].

Corrosion-Fatigue

Half of the corrosion fatigue stress sources are mechanical stresses. It is important to mention that the source of the rest 45%, is caused by externally applied loads, like resonance and/or vibrations from machinery, contraction, or expansion because of temperature cycles or light water hammer [3,41]. Apart from systems operating cyclically, failures can be observed by rapid start-up or shutdown procedures [43].

Corrosion fatigue can be identified by the presence of parallel cracks, lack of crack branching, and the transgranular nature of cracking [42].

Overheating is a crucial parameter that could lead to corrosion fatigue. The presence of a thick deposit, rich in Sulfur or Magnesium, creates graphite nodules and spheroidized Fe_3C

particles accelerating the mechanism even further [43]. Tube bundles in domestic hot water storage tanks are susceptible to this mode of failure [3]. Another factor that has been observed expediting corrosion fatigue is the presence of chloride in the electrolyte. In fact, in many cases, the primary cause that leads to the ultimate fracture is the existence of a chloride-containing corrosive environment [44].

In case copper-zinc alloys have been used, their natural tendency of low fatigue resistance in cooperation with the existence of chloride ions in aqueous solutions results in a mechanically weak copper-rich layer. Areas, where dezincification has occurred, are prone to the initiation of cracks and their propagation because of the corrosion fatigue mechanism [42].

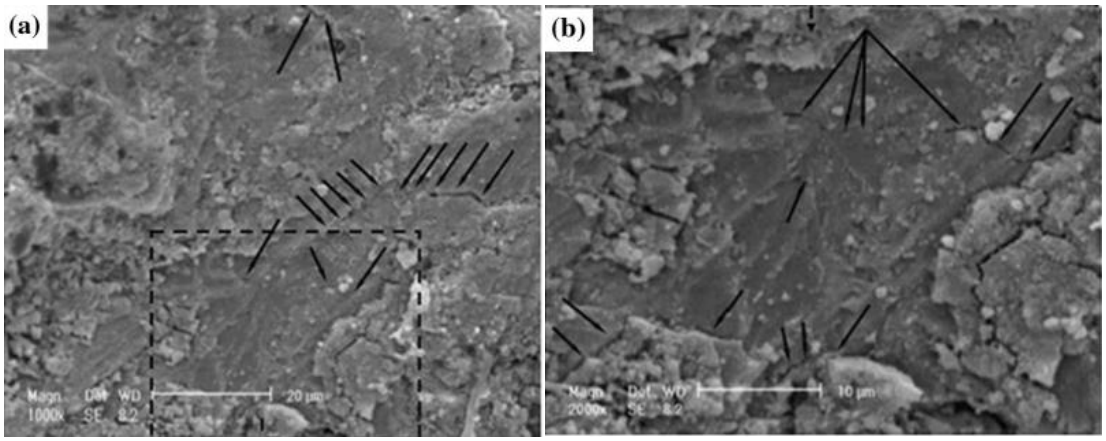

Figure 2-12: SEM micrographs of the fracture surface of a failed tube in secondary electron mode (SE) showing the morphology of the corrosion fatigue cracks and the mode of the crack propagation through the metal [44].

2.3.3 Fouling

Fouling causes build-up on the surface of heat exchangers and this build-up reduces the heat transfer between the fluids making the heat exchanger less efficient. Reducing the efficiency increases fuel consumption and energy loss [45,48]. Fouling takes place for various reasons but it primarily depends on the fluid inside the heat exchanger and the environment in which the device is placed [45]. It has been proven that as fluid temperature decreases, the fouling rate rises. The significance of temperature is independent of the type of fouling [47]. When shearing forces are at their lowest, fouling begins at the end of the tubes and spreads to the circumference as a result of particle transport to the previously deposited particles [48].

Precipitate fouling- Scaling

In heat exchangers running hard water, fouling can occur because of mineral deposits [45]. The solubility of these minerals is influenced by internal forces and temperature alterations.

Precipitate fouling or scaling takes place due to the precipitation of water-soluble salts on the heat transfer surface. The rate of precipitation decreases as find velocity increases. The ability of the tube material to tolerate the erosive effects of fluid velocity must be matched with the fluid velocity [3,45]. Associated with scaling is the existence of suspended solids, mostly in the form of iron, silt, sand, or other visible particles inside the fluid (such as cooling water), which in combination with low velocities can lead to failure [3]. Correspondingly dangerous are high velocities striping away the protective films from the tube surface [46]. When the metal surface temperature is high, solid particle deposition is encouraged, while the induction fouling time decreases [47].

Corrosion-based fouling

Heat exchangers transporting chemicals undergo corrosion-based fouling [45]. In overheated equipment, ammonium chloride-based under-deposits corrosion is frequently documented [17].

Biofouling

The third type is called biofouling. The fluid that is being transported may have living organisms in it. These organisms can stick to the heat exchanger's walls, reproducing and forming their own environment [45]. On numerous occasions, the conditions inside the heat exchanger encourage the quick growth of algae or other marine growths, which obstruct flow and slow down heat transmission.

This type of failure mechanism is common in marine heat exchangers. Marine growth such as algae, marine invertebrates, or aquatic weeds place a coating or film on the surface of the heat transfer tubes. The film functions as an insulator, limiting heat transfer and safeguarding corrodents. This insulating action raises the temperature of the tube walls and accelerates corrosion [3].

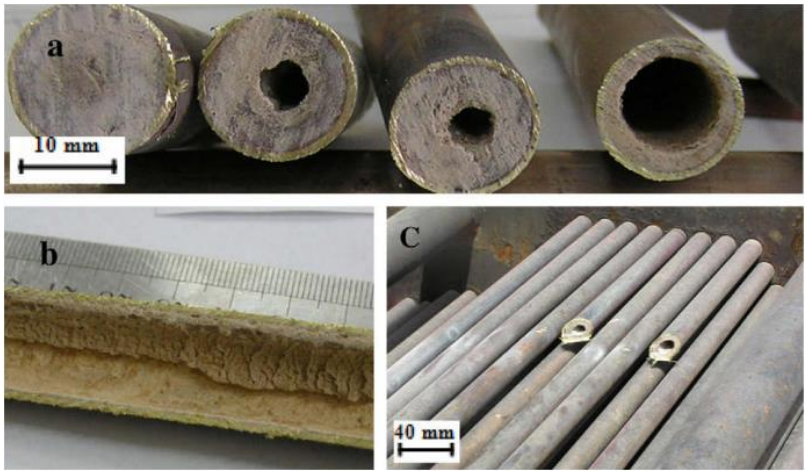

Figure 2-13: Different views of fouling deposition inside the tubes: (a) complete clogging and reduction of internal diameter, (b) sectioned tube, and showing deposition inside the internal surface, and (c) randomly selected tubes, in tube bundle and away from tube sheet inlet. It clearly shows a reduction in internal diameter due to deposition [17].

In the design of heat exchangers, fouling factors are calculated. As the name suggests, it is a factor that needs to be considered over some time [49]. Given that heat exchangers work for an extended period, there might be cases when the internal diameter or the internal cross-sectional area of a pipe will get reduced due to the deposition of particles. There are three main reasons why the particle might get deposited to the inside of a tube, involving scaling by imparities in the fluid, a chemical reaction between the fluid and the wall material, and finally rust formation. The fouling factor is a measure of the resistance to heat transfer caused by the formation of a fouling layer on the heat exchanger's tube surfaces. The fouling factor, also known as Rf or Rd, is a numerical figure that, when compared to the transfer coefficient of a heat exchanger that hasn't been fouled, represents the thermal resistance of the deposit. Numerous common liquids and gases, including fuel oil, saltwater, and alcohol vapor, have standard values accessible. However, to get an accurate result for many materials, including those with the highest fouling factors such as sludges, it is best to do a substance analysis [50].

2.4 Causes of Failures

2.4.1 Structural

Structural root causes involve issues that affect the exchanger’s structural integrity. They involve welding defects, inadequate support, and alignment, mechanical damage, imperfections during manufacturing or secondary manufacturing, and consideration of thermal expansion characteristics.

Welding defects

Welding is used in heat exchangers to join components. However, it produces metal with an inhomogeneous microstructure between the joints. At this point, a dendritic structure (cast metal) and a zone between the heat-affected and the unaffected base metal form the weld. An escalation of metallurgical properties occurs from unaffecting base metal to heat through a heat-affected zone to weld metal. In addition to the welding mechanism, welding could result in the creation of slag or oxygen inclusions, porosity, shrinkage cracks, voids, roughness, poor penetration, and discontinuities. Another potential danger is the rough surfaces that many welds have and their joint with a base metal might be with an undercut or reinforcement [7,17]. Microcracks and porosity often appear in the heat-affected zone and the weld deposit. When the latter is subjected to hydrogen attack cracks appear mainly in the center line or the interface of columnar grains as a result of gas entrapment during solidification [11]. When different materials with different properties are combined, dissimilar welds occur that are prone to unanticipated failures. Failures are enhanced by inappropriate heat treatment and the presence of mechanical stresses. Weld failures are in many cases related to sulfide-assisted corrosion cracking, especially when high weld hardness levels and local dilution of chemistry exist. Steep hardness changes between the two welding materials and tensile residual stresses tend to facilitate weld cracking [59]. In heat exchangers, weld joints are less resistant to misalignment and cyclic loading. The first one results in a non-parallel gap of the brazing joint and when combined with stress concentration leads to failure [17]. Cracking is usually initiated at the root of the welds and their propagation is affected by the mechanical and microstructural properties of the heat-affected zone, as well as high residual tensile stresses and high mechanical service loads [60].

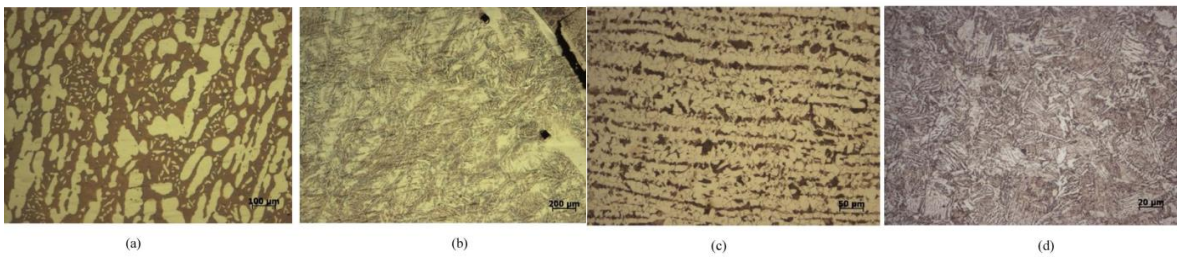

Figure 2.4-1: Microstructure of dissimilar weld: (a) austenite and ferrite duplex stainless steel; (b) dendritic weld microstructure; (c) banded ferrite-pearlite carbon steel; (d) martensite on HAZ of carbon steel [59].

Manufacturing

Second manufacturing such as tube straightening/bending, or cleaning is a more severe source of failures than surface and subsurface imperfections that occurred during primary manufacturing. This issue intensifies since problems from second manufacturing are often overlooked in inspection procedures and specifications. The level of bending stresses that the tube can withstand is determined by operations like straightening, heat treating, and drawing. In case these operations are not followed as they should low residual stresses or high residual stresses near the yield strength of the metal might be produced [7]. Residual stresses appear to be a result of processes such as bending or rolling or even during primary manufacturing [11].

The condition of oxides on the inner surface is immediately affected by cleaning, pickling operations, and control of heat-treating atmospheres. Tubes are prone to pitting corrosion when fractures in the oxide layer create cathodic and anodic sites. If the oxide film has to be removed, cleaning must remove it all so that no anodic and cathodic sites are established [7].

Inadequate support and alignment

Tube support plates and tube sheets that are not aligned properly reinforce the creation of stresses induced during fabrication [7].

2.4.2 Operational

Working parameters

Working parameters are a major root cause that leads to failure due to fatigue mechanisms. It is expressed in two ways: thermal overload and mechanical overstress [11].

Elevated temperature

Unexpected embrittlement of any material at or above the service temperature failing the component occurs due to the effect of elevated temperatures on weak materials. Metallurgical changes could potentially be caused by embrittlement leaving the material brittle at room temperature and ductile and tough at elevated temperature. When materials with different thermal coefficients and/or compositions are found together thermal cycling failures are a possible threat. Excessive temperatures could also lead to creep and stress rupture, scaling, and oxidation [7].

Environment

Failures and specifically cavitation erosion of plain carbon steel have been observed in an SO_2 vapor environment. The entrance of cold SO_2 in the heat exchangers and its boiling can result in cavitation erosion and subsequent metal loss [62].

2.4.3 Metallurgical

Phase transformation

A common metal used in heat exchangers is stainless steel due to its metallurgical properties, such as high ductility, excellent corrosion resistance, good formability, high mechanical properties, and heat resistance. Another stainless-steel property is their metastability, which allows them to undergo a phase transformation, by plastic deformation under monotonic or cyclic loading or deep cooling, from austenite to martensite. This transformation can be induced by stress, strain, or temperature. However, this transformation breaks the passive film, due to the martensite volume expansion creating residual stresses and different corrosion potentials. The last leads to the creation of an anode and a cathode resulting in galvanic corrosion [61].

2.4.4 Design issues

Stress concentration in many heat exchangers is due to their shape which is producing vulnerable regions. Design considerations, such as the coefficient of thermal expansion and yield strength at high temperatures, influence the lifespan of mechanical joints. In case the materials in the assembly have very different thermal coefficients then a tension of relaxation is created, permitting leakage [7].

Various design parameters influence fouling, as well as the rate of this failure mechanism. One important factor is the structure of the surface. Since the inner surface of heat exchangers is usually enhanced to increase thermal resistance, accelerating the fouling process also affects it. At the same time, scale formation is easier and faster on textured surfaces rather than smooth ones. Dead areas also create fouling risks [11].

2.5 Types of Inspection

The integrity of heat exchangers can be impacted by several degradation processes, which can lead to costly repairs, tube blocking, or bundle replacement. Inspection and monitoring for the identification and characterization of the degradation is one important aspect of ensuring tube integrity [51]. There is no single non-destructive technique that can be used to inspect all heat exchangers. The advantages and limitations of each technique should be

taken into consideration before they are applied. Proper testing and selection of inspection methods lead to accurate and reliable results [57]. The following are a few of the well-known heat exchanger inspection methods: Laser Inspection, Ultrasonic Testing (UT), Internal Rotary Inspection System (IRIS), Remote Field Testing (RFT), Remote-Field Array (RFA), Near-Field Array (NFA), Radiographic Testing (RT), Eddy Current Testing (ECT), Acoustic Emission Testing (AET), Near-Field Testing (NFT), Infrared Thermography (IRT), Magnetic Flux Leakage (MFL), Tangential Eddy Current Array (TECA), Eddy Current Array (ECA), Transverse Field Inspection (TFI) and Partial Saturation Eddy Currents (PSEC) [58]. Some of the above methods are briefly presented in this chapter.

2.5.1 Eddy current testing

Eddy current testing (ECT) is one of the most common techniques used in the non-destructive field. Bobbin coils are typically used for in-service inspection of heat exchangers because they are effective at detecting volumetric degradations. However, specific probes are needed for the identification and measurement of additional forms of degradation including pitting, intergranular attack (IGA), axial cracking, and circumferential cracking [51]. When applying the eddy current testing concept, a single coil is activated by alternating electrical currents. A magnetic field is created around the coil when the wire is excited. The frequency that goes through the coil is the same as what the electromagnetic field oscillates at eddy currents, which are opposite to the coil's currents produced when the coil is exposed to the conductive material. When everything is in order and a conductive material is introduced to the magnetic field, they continue to flow in a stream-like pattern around the coil, forming the EC System. These streams begin to leap off the conventional eddy-current magnetic field if the conductive material has defects, breaks, or cracks, changing the voltage that you are monitoring. These variations in conductive materials may be quantified for fault detection, enabling us to find problems even when the eye cannot [52]. Critical detection concerns at vulnerable locations, such as the tube sheets rolled-joint transitions, U-bends, and tube-support intersections, can be resolved by this EC technology [51].

2.5.2 Internal Rotary Inspection System

Internal rotary inspection system (IRIS) is an ultrasonic system mainly used in air-cooled heat exchangers where corrosion occurs at the bore surface, and belongs in the non-destructive technology. IRIS is based on an ultrasonic pulse-echo immersion technique, measuring the wall thickness and displaying the measurements in a pattern that depicts the tube's circumferential cross-section. The necessary equipment involves the test head and

probe drive mechanism, the water supply regulator and deionizer, and the oscilloscope and associated electronics chassis [53]. For IRIS to work the surface needs to be cleaned so that dust, internal deposits, loose foreign particles, or contaminants are removed. The final step before the inspection begins is tube identification to achieve full traceability. During the inspection procedure, the test head is connected to the water supply kit, starting at the end of the tube and pulling gradually to the start. The pulling speed is between 30-50 mm/s and depends on the rotating speed of the turbine. The ideal results involve a rectangular picture on the oscilloscope [54].

2.5.3 Visual inspection with a videoscope

Videoscopes are used to inspect the inner surfaces of tubes, so remote visual inspection (RVI) is perfect for difficult-to-access areas. Videoscopes can record both static and moving images thanks to a tiny sensor chip in the tip of their insertion tubes. An inspector can observe these photos on an LCD screen thanks to the sensor, and use a videoscope to observe what a fault looks like inside the heat exchanger tubes. The height and depth of corrosion inside the tubes can also be measured. To help inspectors comprehend the scale and shape of corrosions even better, some equipment offers 3D modeling [55].

2.5.4 Magnetic flux leakage

Small-bore ferromagnetic heat exchanger tubes can be inspected using the electromagnetic technique known as the Magnetic Flux leakage (MFL) technique. A magnet with two different sorts of pickups—a coil type and a Hall element—makes up the MFL probe. Coil-type sensors detect the flux rate of change, whereas Hall-type sensors detect flux absolute. Small flaws that induce flux alterations are found in the coil. The MFL instrument measures the output voltage that the rate of change of flux induces (Faraday's Law). The gradual wall loss is identified using the Hall-element sensor. While the defect size is unrelated to the output of the MFL coils, the flaw's effect on flux is. Wall loss-type faults can be sized using the Hall Element [56]. Although MFL involves many advantages it cannot be used in U-bend tubes, detectability is limited to laws more than 20%, longitudinal or axial flows cannot be detected as well and size discontinuities cannot be sized accurately [57].

2.5.5 Laser optic

The optical triangulation idea is used in this examination technique. The probe used in laser-based surface mapping devices projects a tiny laser beam onto the surface of the tube and works like a "laser caliper," measuring the internal dimensions of the tube rather than just

detecting a fault. A precise and quantitative map of the interior surface topography is produced by rotating the laser sensor while the probe is drawn through the tube. On the target surface, a brief light beam is directed at almost normal incidence. This light spot is imaged by receiving optics onto a single-axis lateral-effect photodetector. Changes in target proximity are translated into lateral movement on the photodetector because receiving and transmitting optics are at different angles. The depth of a pit is equal to the displacement of the light spot on the detector. Advantages of this method include the capacity to inspect approximately 18 tubes, with the ability to permanent records in real-time inspections with thousands of data point samples. Some limitations that need to be taken into consideration are the inability to inspect new stainless-steel tubes due to the mirror-like effect as well as the inability to provide wall thickness measurements [57].

2.6 Assessing the Impacts

Failures in heat exchangers don't affect only the reliability and efficiency but they also have severe implications concerning the safety and the economy of the industry. Assessing the impacts in those aspects is important to make the proper decisions about maintenance strategies, risk management, and design improvements.

In an investigation conducted by NACE Impact, the global cost of corrosion is estimated to be 2.5$ trillion US dollars. Financial impacts involve maintenance expenses, increased operational costs, and production losses. Referring to production losses, as the main purpose of heat exchangers is heat transfer, failures reduce their efficiency, decreasing at the same time production rates. Downtime, shutdowns, or reduced throughput are factors that need to be taken into consideration while estimating the economic impact. Since a heat exchanger is not working properly the energy it needs is relatively increased to maintain the desired temperatures. At this point, understandably, maintenance and repair produce an extra cost, requiring repair or replacement of components, additional chemical programs, new materials, maintenance equipment, and labor hours. Additional costs that in most cases are not taken into consideration are unnecessary inspections, installation, and delivery costs.

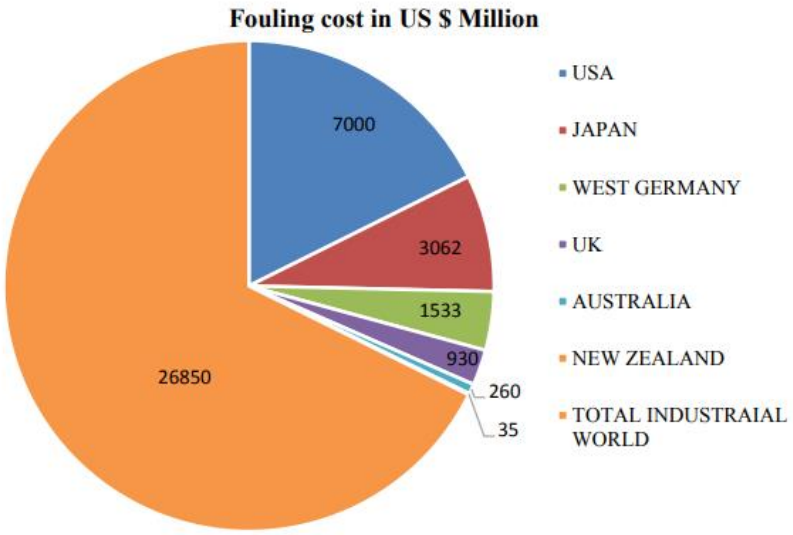

Figure 2.4-2 Fouling costs based on estimations [11].

Failures can also create safety hazards, where accidents, potential injuries, and fatalities create an unfriendly and dangerous environment. At the same time, environmental releases that will require environmental clean-up appear to be an important aspect that affects both safety and the economy.

Adapting the proper maintenance strategies and implementing the right design improvements will ultimately improve the operational processes of heat exchangers, providing a safe and sustainable environment.

3. HEAT EXCHANGER FAILURE: CASE STUDIES SUMMARY AND PRESENTATION

3.1 Failure study of a. Sea exchanger tube and b. Flexible EADC transport pipeline

Introduction: A refinery commissioned the Materials Laboratory of the University of Thessaly (LoM) to study the failure of parts of the refinery's equipment specifically the failure of a sea exchanger tube and a flexible EADC pipeline. The sea exchanger tube failed due to erosion-corrosion and the pipeline due to pitting corrosion. Laboratory tests involved visual inspection using a stereo-optical microscope, metallographic analyses, microsclerometers, and the use of a scanning electron microscope (SEM).

Material Selection: The tube of the sea exchanger was made of Cu alloy according to ASTM specification B111-687. The pipeline was made of stainless steel, used to transport ethyl aluminum dichloride (EADC).

Stereo-optical microscope: Referring to the tubes' failure the presence of areas with individual craters of ellipsoidal morphology and abrasion lines from the solid particles at the seawater circulating within the tubes led to the spread of the corrosion. Wall thickness is gradually reduced due to erosion-corrosion leading to tubes' perforation. At points where craters are more and deeper, corrosion is more intense.
Referring to pipelines' failure stereoscopic inspection shows the area of the flexible tube perforation, which is toward the highest part of the conduit configuration. Scratches are observed on the pipeline which are probably due to the steel that surrounds it for protection. From the check made in the stereoscope, there does not seem to be another area with a similar problem.

Metallography: Referring to the tubes' failure metallographic analyses showed that the corrosion started from the inner surface, while the outer was corrosion-free, and that the microstructure of the material consisted of a solid solution Cu-Zn.
Referring to pipelines' failure metallographic analysis showed that pitting initiated from the inner surface.

Micro sclerometer:
Referring to the tubes' failure the microhardness of the tubes was measured in profile from the inner to the outer surface. It is observed that the values are stable approximately 99 $HV_{0.2}$.

SEM analysis: Referring to the tubes' failure SEM analysis showed deposits of $CaCO_3$, SiO_2, and MgO.

EDX analysis: Referring to pipelines' failure according to Energy Dispersive X-ray analysis (EDX), the microstructure of the material is austenitic, with a significant concentration of chloride in the hole area. This increased concentration with the simultaneous presence of residual stresses led to pitting corrosion. An important remark about this particular failure is that it occurred only in one spot which leads to the conclusion that a possible material defect (e.g. a large inclusion) contributed to the failure.

Conclusions: Referring to the tubes' failure, in summary, the results of the analyses showed the following:
(1) Formation of corrosion craters with an ellipsoidal morphology inside the exchanger chambers. The ellipsoidal morphology indicates a mechanism of mechanical erosion (erosion-corrosion), where at the same time as the erosion, a mechanism of wear by materials carried in the flow of seawater operates.

(2) The thickness of the tube gradually decreases, due to mechanical erosion, and leads in some cases to the perforation of the tubes.
(3) Analyzes of the deposits showed that they are composed of CaCO3, SiO2, and MgO.
(4) The phenomenon does not develop uniformly but has a local character. There are areas where mechanical erosion is more intense, as shown by the number and depth of the craters.
According to the above, the failure mechanism is mechanical corrosion by entrained materials in seawater.
Referring to pipelines' failure to summarize, the above results are summarized as follows:
(1) The perforation of the flexible pipe started from the inside and it was caused by pitting.
(2) The pitting was caused by the formation of a microenvironment with an increased chlorine content.
From the inspection of the section of the pipeline, it appears that this perforation is an isolated event since the rest of the section did not present corresponding problems. Therefore, it is possible that some possible material imperfection (e.g. some large inclusion) contributed to the failure. This imperfection, if it existed, could not be determined since it was removed during the corrosion process.

3.2 Corrosion study of E-1103B exchanger tubes

Introduction A refinery commissioned the Materials Laboratory of the University of Thessaly (LoM) to study the corrosion of heat exchangers' E-1103B tubes. The failure took the form of pits and larger openings longitudinal to the main axis of the yards. Laboratory tests involved the use of stereo-optical microscopy, metallographic analysis, and the use of a scanning electron microscope (SEM).

Material selection: The tube was made of SANICRO 28 according to the company SANDVIK (Cr: 27%, Ni:31%, Mo:35%).

Operational conditions:

	Shell Side			
▶	Un-stabilized Naphtha	Mixture: C1 - C4 & C5 - 175oC & H2S & H20		
▶	Temp inlet (oC)		Average:	157
▶	Temp outlet (oC)		Average:	130
▶	Average ΔT (oC)			27
▶	Press inlet (Kg/cm2 g)		Average:	2,2
▶	Temp outlet (Kg/cm2 g)		Average:	1,6
▶	Average ΔP (Kg/cm2 g) - [Δ (C-1101 - V-1102)]			0,6
▶	Chemical Treatment	*Salt Dispersant & Neutraliser Inhibitor*		
▶	Water (from stripping steam at C-1101 @ MT/H)		Average:	9,4
▶	Water at C-1101 Overhead (%Wt)		Average:	4,6

Table 3-1: The operational conditions on the shell side.

The environment on the shell side (acidic - corrosive agents HCL etc.) at the top is affected - corrected by the use of chemicals (and changes daily). The aim is to keep it constant in the specifications. The final naphtha is considered max 165ºC (ASTM 30-165ºC).

Stereo-optical microscopy: The outer surface of the tubes is covered by deposits/corrosion products that locally have an approximately round shape and protrude from the outer surface of the tube. Visually, layering of the corrosion products is observed.
Metallography: The inner surface (ID) is clear of corrosion, but on the OD, in addition to the reduction in thickness, pitting corrosion is observed.

SEM/EDX analysis: An area from the outer surface of the tube was analyzed with a scanning electron microscope. The purpose was to study the morphology of these areas - the evolution of which leads to perforation of the tube -, as well as to determine their composition with EDX. The uncorroded region consists of Fe:40%, Cr: 30%, and Ni: 30%.

Conclusions: Based on the results of the laboratory tests, as well as the study of the available open bibliography we come to the following conclusions:
The failure of the tubes starts from the outer surface (shell side) where a high S, Cl content is found in corrosion products. The presence of H_2S in the stream of naphtha on the shell side causes local corrosion with the formation of pyrrhotite FeS1.15. The pyrrhotite film is porous and cathodic concerning steel, creating galvanic corrosion conditions. At temperatures above 150ºC and especially with the presence of chlorides, a $FeCl_2$ film is formed which hinders the formation of pyrrhotite. $FeCl_2$ is acidic (due to the hydrolysis of iron) and maintains an intense corrosive action under the pyrrhotite film, leading to pitting

and perforation of the tube. This corrosion mechanism has been called barnacle-type corrosion.

3.3 Failure study of E7114 exchanger tube

Introduction: A refinery commissioned the Materials Laboratory of the University of Thessaly (LoM) to study the corrosion of heat exchangers' E-7114 tubes. The tubes were put into operation in June 2010 and developed a leak in February 2012. Laboratory tests involved the use of stereo-optical microscopy, chemical analyses, metallographic analyses, micro sclerometers the use of a scanning electron microscope (SEM), and Energy Dispersive X-Ray Analysis (EDX).

Material selection: The material of the tube meets the requirements of the specification ASTM A335 grade P regarding its chemical composition.

Operational conditions:

DESIGN DATA

SIZE	685 I.D x 6096 L		TYPE	H-AES
CODE	ASME SEC. VIII DIV.1 '2007 ED. PED 97/23/CE		TEMA CLASS	"R"(8TH. ED.)
SURFACE AREA	111.0 M^2		NO. OF SHELL	1
CODE STAMPING	NO	SHELL SIDE	TUBE SIDE	UNIT
FLUID NAME		CRUDE	LGO	-
DESIGN PRESSURE (INT'L /EXT'L)		36.7[3.599] / -	28.3[2.775] / -	KG/CM2.G [Mpa.g]
OPERATING PRESSURE		16.9[1.657] / -	9.0[0.883] / -	KG/CM2.G [Mpa.g]
DESIGN TEMPERATURE		210	290	℃
OPERATING TEMPERATURE (IN/OUT)		176.9 / 181.7	260.3 / 186.4	℃
HYDRO. TEST PRESSURE		52.48[5.147]	40.47[3.969]	KG/CM2.G [Mpa.g]
PNEUM. TEST PRESSURE		-	-	KG/CM2.G [Mpa.g]
CORROSION ALLOWANCE		3.0	6.0	MM
POSTWELD HEAT TREATMENT		NO	YES (SEE NOTE-1)	-
STRESS RELIEF		YES(HEAD ONLY)	NO	-
RADIOGRAPHY (S/H)		SPOT / FULL	SPOT / -	-
JOINT EFFICIENCY (S/H)		85 / 100	85 / -	%
INSULATION		90 (H.C)	100 (H.C)	MM
NO. OF PASS		1(ONE)	8(EIGHT)	-
MIN. DESIGN METAL TEMPERATURE		-4	-4	℃
M.A.W.P		36.7[3.599]	28.3[2.775]	KG/CM2.G [Mpa.g]
M.A.E.P		-	-	KG/CM2.G [Mpa.g]
WIND CODE		AS PER SPEC.		-
EARTHQUAKE CODE		EAK2000		-

NOTE : 1. The heat treatment shall be applied to Channel & Float. Head and flange.

Table 3-2: The design data of the heat exchanger.

Chemical analysis: Chemical analysis was performed on the tube material. The comparison shows that the material of the yards meets the requirements of the specification.

	C	Si	Mn	P	S	Cr	Mo
Χάλυβας αυλού E7114	0.1	0.35	0.41	0.01	<0.01	4.8	0.51
ASTM A335 P5	0.15 max	0.5 max	0.3-0.6	0.025 max	0.025 max	4-6	0.45-0.65

Table 3-3: The results and the relevant specification requirements.

Stereo-optical microscopy: On the outer surface of the tubes, there is a layer of corrosion products/sediments. Intense pitting corrosion is observed, which has locally developed and led to the perforation of the tubes.

Metallography and micro sclerometers: Metallographic analysis and the use of micro sclerometers were used in two different specimens, one longitudinal and one transverse to the main axis of the tube. Concerning the longitudinal specimen, they showed that corrosion initiated from the outer (OD) to the inner (ID) surface, with deposits and corrosion products accumulating inside pits increasing the corrosion rate depending on the microenvironmental conditions. The microhardness of the is approximately 161 $HV_{0.3.}$ Concerning the transverse specimen, the microstructure of the tube consists of ferrite and spheroidized carbides. In this sample, intense pitting corrosion is observed in the OD with the creation of sharp pits, the development of which leads to perforation of the tube. No corrosion is observed on the inner surface (ID). The microhardness of the sample is approximately 170 $HV_{0.3}$.

SEM and EDX analysis: SEM and EDX analysis were used to determine corrosion products and the results indicated a high concentration of S (25-40% wt.).

Conclusions: Summarizing the results of the laboratory tests presented in the previous paragraphs:

(1) The material of the tube meets the requirements of the ASTM A335 specification grade P5 in terms of chemical composition.

(2) The tube microstructure consists of ferrite and spheroids carbides with microhardness 161-170 $HV_{0.3}$.

(3) The corrosion problem starts from the outer surface (shell side) and develops into perforation.

(4) Corrosion products/deposits on the exterior accumulate at the interior of the pits and contain locally very high amounts of S (25-40% by weight), but without a continuous protective film of sulfides having formed. At the same time, in the same areas, Cl is found in percentages of 2-5.9% wt., and portable materials such as Ca, Al, and Na.
(5) The leakage was observed in less than 2 years, which indicates an erosion rate locally of ~ 1.65 mm/y.
Due to the absence of a continuous protective film of Fe sulfide, the corrosion morphology in the form of pitting, and the locally high rate of corrosion the morphological features of the corrosion refer to corrosion due to the presence of naphthenic acids (naphthenic acid corrosion, NAC). The development of this type of corrosion is influenced by factors such as the content of crude oil in naphthenic acids (NAP), the content of argon to sulfur, the temperature and flow rate of the argon as well as from the construction materials. It is pointed out that although the content of naphthenates of acids in crude oil is given by the TAN number (Total Acid Number), TAN generally expresses the mineral acid content of the argon and it has been found in the literature that crude oil with the same TAN can give
different rates and types of corrosion because the content of naphthenic acids (even for the same TAN) is different. In this case, the TAN of crude has low values, but given the relatively stagnant flow conditions reported by the refinery, which may locally affect TAN as well as the content of argon in naphthenic acids, as well as its morphology corrosion, the failure of the ducts is attributed to corrosion due to presence naphthenic acids.

3.4 Study of causes of corrosion of E-7528 exchanger tubes

Introduction: A refinery commissioned the Materials Laboratory of the University of Thessaly (LoM) to study the corrosion of the heat exchanger's E-7528 tubes. Two corrosion mechanisms were detected, under deposit corrosion with the presence of chlorides on the tube side and ammonium bisulfite corrosion on the shell side leading to a decrease in the thickness of the tubes. The tubes were replaced after 8 years of operation due to corrosion problems. Laboratory tests, of 3 different specimens with different corrosion rates, involved the use of stereo-optical microscopy, chemical analyses, metallographic analyses, micro sclerometers the use of a scanning electron microscope (SEM), X-ray diffraction (XRD), and Energy Dispersive X-Ray Analysis (EDX).

Material selection: According to the manufacturer the tubes were made of steel SA 210-A1.

Operational conditions: According to the refinery, a mixture of H_2+H_2S+H+H_2O+NH_3 circulated on the shell side, while cooling water circulated on the tube side. The temperature (operational data) is 84ºC /41ºC (inlet/outlet, shell side) and 32ºC/41ºC (inlet/outlet, tube side). The analysis of the cooling water in 3 phases (before leakage, during leakage, and after restoration) is given in the table below.

Parameter	Units	Prior Upset	During Upset	Recovery phase
pH		7,9	6.5 - 9.5	8
Specific cond.	µs/cm³	250	1000 - 2000	650
TH	ppm $CaCO_3$	45	141 - 300	52
M-Alkalinity	ppm $CaCO_3$	55	5	85
Total - OPO4	ppm PO_4-	0,74	5,9	12,5
Filtered- OPO4	ppm PO_4-	0,45	4	10,9
T-Zn	ppm Zn+	1,45	0	0,85
Total -Iron	ppm fe++	0,78	1,4	7,8
Iron - Soluble	ppm fe++	0,2	1,1	5,2
Chlorides	ppm Cl2	47	32	57
SO4	ppm	N/A	730	110

Table 3-4: The analysis of the cooling water in 3 phases.

Chemical analysis (wt.%): Chemical analysis was performed on the tube material.

	C	Si	Mn	P	S
E -7528	0.18	0.19	0.62	0.02	0.01
SA210-A1	0.27 max	0.1 max	0.29-1.06	0.035 max	0.035 max

Table 3-5: The results and relevant specification requirements.

Stereo-optical microscopy: The tubes that were "grouped" as A show intense corrosion on their entire outer surface with characteristic spots whose center is black and around it accumulates corrosion products with a yellowish color. The tube characterized as B presents a smaller extent of the above phenomenon in terms of the extended appearance of the yellowish color, while in tube C, two distinct areas are observed along the main axis, one of which refers to phenomena corresponding to those of category A, and the other in phenomena corresponding to B.

Metallography: Metallographic analysis showed that corrosion on both specimens A and B initiated from both the inner and the outer surface of the tubes since deposits were found on both, while on specimen C it is more intense on the inside. On the inner surface, the problem

appears to be more severe with erosion progressing to pitting corrosion under the layer of corrosion products (under deposit corrosion).

Micro sclerometer: The values are relatively uniform and no noticeable difference is observed in the samples measured.

SEM/EDS and XRD analysis: Corrosion products were determined with the use of SEM/EDS and XRD analysis where a high concentration of S was observed on the shell side and a large number of corrosion products with a strong presence of Cl at the corrosion products/steel interface, on the tube side.

X-ray diffraction: Regarding corrosion on the tube side, the compounds identified based on X-ray diffraction are: sulfur (S), and iron oxides (Fe_2O_3, Fe_3O_4) and the mechanism evolves as:

1. Formation of deposits.
2. Infiltration of Cl beneath the deposits and formation of MCl.
3. Hydrolysis of MCl and formation of HCl: $MCl+H_2O \rightarrow MOH+HCl$.
4. pH reduction and autocatalytic corrosion.

Regarding the shell side Fe, O, and S were detected and XRD analysis identified the compounds as sulfur (S), iron sulfides (FeS_2, FeS), iron oxide (Fe_2O_3), and ammonium bisulfide NH_4HS.

Conclusions: Summarizing the results of the laboratory tests:

(a) From the laboratory results it is clear that two corrosion mechanisms operate simultaneously, the first on the outside of the tubes (process gas side) and the second on the inside of the tubes (cooling water side).

(b) Both mechanisms lead to a reduction in tube thickness. However, the strongest reduction in thickness is due to the mechanism that develops inside the tubes (cooling water side).

(c) Corrosion inside the chambers is defined as under-deposit corrosion in the presence of chlorides. The mechanism evolves as follows:

(1) Deposit formation.

(2) Cl infiltration beneath the deposits and formation of MCl.

(3) Hydrolysis of MCl and formation of HCl: MCl+H2O→MOH+HCl.

(4) PH reduction and autocatalytic corrosion.

(d) Corrosion on the outside of the chambers is defined as ammonium bisulfite corrosion. This corrosive acid salt results from the H2S+NH3 reaction present in the process gas.

3.5 Evaluation of the cleaning of the internal surface of the E-3310 exchanger

Introduction: A refinery commissioned the Materials Laboratory of the University of Thessaly (LoM) to evaluate the degree of cleaning of the inner surface of the exchanger E-3310. Three specimens were examined, two of them before getting cleaned and the third after the cleaning process, with a pressure of 2000 bar. Laboratory tests the use of stereo-optical microscopy, metallographic analysis, the use of scanning electron microscope (SEM), and X-ray diffraction (XRD).

Material selection: According to the manufacturer the tubes were made of stainless steel 410.

Visual inspection and metallography: Visual inspection and metallography showed a layer of corrosion products/deposits accumulated on the inner surface of the sample before cleaning and the layer disappearing after cleaning.

SEM analysis: Corrosion products were determined using SEM and XRD analysis inside the tubes. SEM/EDS showed that this layer included the elements C, O, S, Si, and Al. Locally the concentrations of these elements were high (Al: 11.18%, Si: 9.18%, S: 14.99%). After cleaning, the above elements were not detected on the inner surface of the tubes.

XRD analysis: XRD showed the presence of the following phases: Al_2O_3, SiO_2, and graphite which are portable materials, $Fe_{1-x}S$, Fe_2O_3, which are corrosion products, and Fe-Cr from the steel.

Conclusions: According to laboratory results, it seems that this coating is created more by portable materials that are deposited inside the tubes and not by a reaction with the surface of the steel. Corrosion products are less than portable materials. This is also confirmed by the fact that no significant corrosion was observed in the steel inside the tubes (only the outside had corrosion). Therefore, the type of alloy does not affect the formation of the coating. The only thing that could affect it is the condition of the tubes' surface. An increased roughness would favor the formation of the coating.

3.6 Failure analysis investigation of tubes from the heat exchangers E-7533 A & B

Introduction: A refinery commissioned the Materials Laboratory of the University of Thessaly (LoM) to study the corrosion of heat exchangers' E-7533 A & B tubes. The outer surface of the tubes from E-7533 A was covered by sufficient quantities of material, which

was mainly brownish in color and easily friable. The thickness of the tubes was checked on-site, and the results showed that more than 50% of the initial thickness was reduced.
The outer surface of these tubes from E-7533B was almost free of thick deposits, and in one of them, a hole existed. According to the refinery, holes have been identified on 7 different tubes of the E-7533B, and most of them were located around the impingement baffle (Cooling water inlet – shell side). The thickness of the tubes was checked on-site, and the results showed that more than 50% of the initial thickness was reduced. Laboratory tests involved chemical analysis, metallographic analysis, the use of stereo-optical microscopy, microhardness testing, the use of a scanning electron microscope (SEM), and X-ray diffraction (XRD).

Material selection: According to the manufacturer, the tube material is steel SA 210 A-1.

Operational conditions:

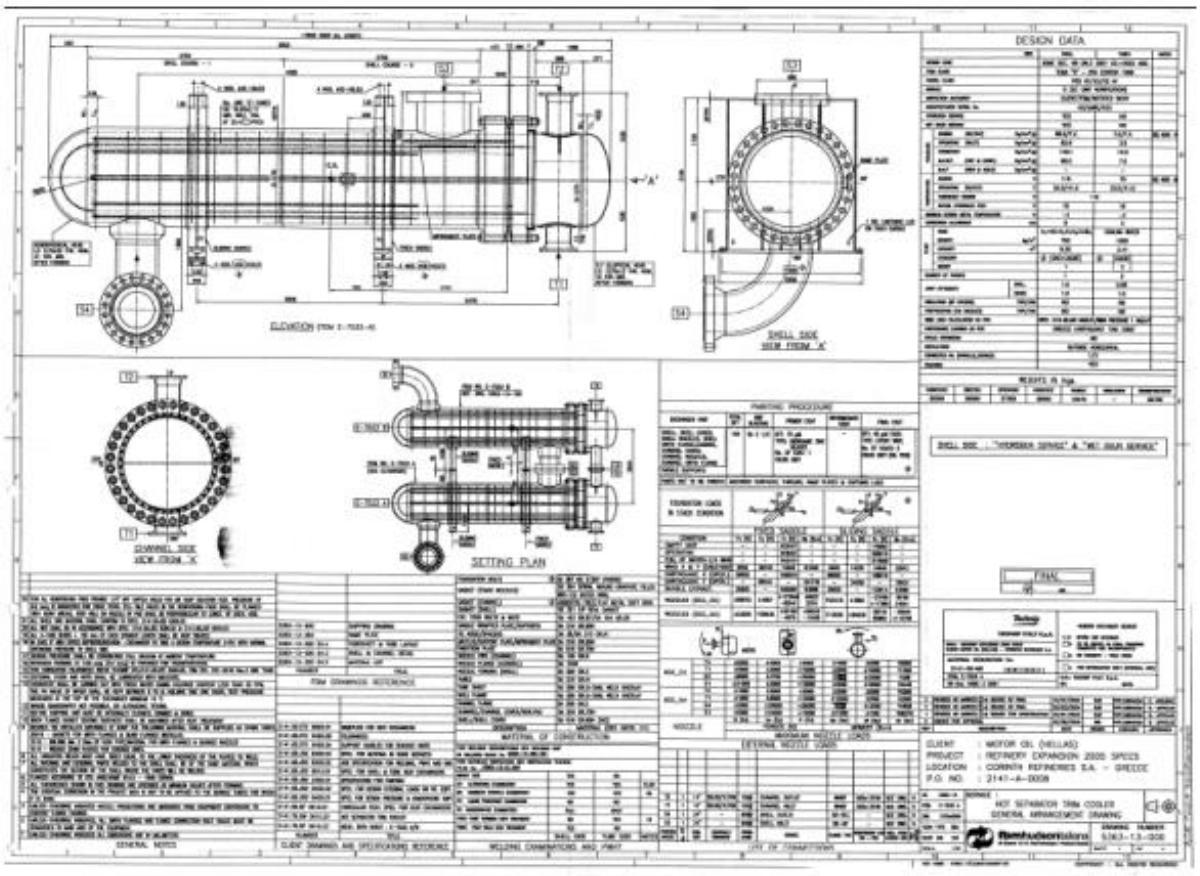

Table 3-6: The design data of the exchangers.

Parameter	Units	Prior Upset	During Upset	Recovery phase
pH		7,9	6.5 - 9.5	8
Specific cond.	µs/cm³	250	1000 - 2000	650
TH	ppm $CaCO_3$	45	141 - 300	52
M-Alkalinity	ppm $CaCO_3$	55	5	85
Total - OPO4	ppm PO_4-	0,74	5,9	12,5
Filtered- OPO4	ppm PO_4-	0,45	4	10,9
T-Zn	ppm Zn+	1,45	0	0,85
Total -Iron	ppm fe++	0,78	1,4	7,8
Iron - Soluble	ppm fe++	0,2	1,1	5,2
Chlorides	ppm Cl2	47	32	57
SO4	ppm	N/A	730	110

Table 3-7: Operational data for the cooling water on the tube side.

	mol %basis	mas % basis
H2	71,24	11,05
H2S	1,81	4,74
NH3	0,16	0,21
H2O	11,12	15,41
MDEA	0,00	0,00
METHANE	7,27	8,97
ETHANE	1,79	4,14
PROPANE	0,88	2,97
IBUTANE	0,24	1,05
BUTANE	0,33	1,48
Heavier HC	5,18	49,97
Temperature degC	23 - 30	23 - 30
Pressure kg/cm2 g	83,60	83,6
Flow in kmol/hr	15240	
Flow in kg/hr		198039

Table 3-8: Operational data for the shell side.

Chemical Analysis (wt.%): The results of chemical analysis carried out on tube material from both exchangers, are given. From the comparison with steel SA 210-A1, it is obvious that the tube material complies with the requirements of the specification.

	C	Si	Mn	P	S	Al
E -7533 A	0,18	0,25	0,82	0,013	0,0023	0.0271
E -7533 B	0,17	0,23	0,79	0,011	0,0031	0.0243
SA210-A1	0.27 max	0.1 max	0.29-1.06	0.035 max	0.035 max	-

Table 3-9: The results of chemical analysis.

Stereo-optical examination: Concerning heat exchanger E-7533 A, stereo-optical examination showed that a thick layer of brownish "material" has accumulated on the outer tube surface. This "material" was friable, could easily be detached, and had completely

covered the whole outer surface of the tubes. In some areas of the outer surface, this layer was porous and it is cracked exposing the underlying steel.

Concerning heat exchanger E-7522 B, the outer surface of these tubes was almost "clean" of deposits in comparison to the case of E7533A. Local thickness reduction can be observed in several areas of the outer tube surface, associated with material removal in layers, a condition that resembles exfoliation-type corrosion. These phenomena concern less than half of the outer surface area. The morphology of the surface corresponds to the morphology reported in our failure analysis investigation of the exchanger E-7528 and is attributed to ammonium bi-sulfide corrosion. Tube perforation was due to a hole with an approximate 6x6 mm opening. There is also evidence that erosion is an assisting mechanism, that contributes to the overall thickness reduction

Metallography- Microhardness measurements: Concerning heat exchanger E-7533 metallography and microhardness testing were performed on two transverse specimens and one longitudinal. Regarding the transverse specimens, local large corrosion cavities were developed at the ID of the tube, which evolved towards the OD, consuming the material, while limited corrosion phenomena were observed at the OD. The friable "material layer", which was observed during the macroscopic examination of the tubes, upon their receipt, remained at the OD but below this layer, only limited corrosion can be observed. The average microhardness values of this specimen are 149 $HV_{0.3}$ (OD), 155$HV_{0.3}$ (center), and 150 $HV_{0.3}$ (ID). Regarding the longitudinal specimen large and local corrosion cavities were formed at the ID, while the OD area seemed to exhibit limited corrosion phenomena. The average microhardness values of this specimen are 149 $HV_{0.3}$ (OD), 140 $HV_{0.3}$ (center), and 155 $HV_{0.3}$ (ID). At the outer surface, S, Ca, and O were detected.

Concerning heat exchanger E-7522 B metallography and microhardness testing were performed on two transverse specimens and one longitudinal. For all three specimens, from the macroscopic view, it is concluded that corrosion phenomena evolved both at the ID and OD areas, however, most of the material removal has taken place on the OD. The main corrosion characteristic at the ID is the local, almost round corrosion cavities, while at the OD thickness reduction seems to be more uniform. It is clear that there is significant thinning of the tube, both from the ID and the OD, but it should be stated that the corrosion mechanism which was dominated at the OD area, proceeded more rapidly. For the transverse specimen average microhardness values are 140 $HV_{0.3}$ (OD), 141 $HV_{0.3}$ (center), and 155 $HV_{0.3}$ (ID),

while for the longitudinal average microhardness values are 135 $HV_{0.3}$ (OD), 148 $HV_{0.3}$(center), 134 $HV_{0.3}$ (ID).

SEM/EDX analysis: Concerning heat exchanger E-7533 A according to SEM/EDX analysis Al, S, Ca, and Si were detected at the inner surface. At the outer surface Fe, S, Ca, and O were detected. In addition, high Cl- concentrations (1% wt.%) were detected at the ID and more specifically at the interface of the steel with the corrosion products.
Concerning heat exchanger E-7522 B according to EDX analysis Al, O, S, Ca, Cu, and Zn were detected. At the outer surface C, Fe, S, O, and Ca were detected.

X-ray diffraction: The brownish friable material collected from the outer surface of the tubes from E-7533A was further analyzed by XRD. According to the XRD spectrum, the following phases have been identified in this "material": S, FeS_2, Fe_2O_3, SO_2, FeS, and SiO_2.

Conclusions: The main experimental results presented above, are summarized below per each case:
E-7533 A: (1) The tubes were completely covered by a friable brownish "material" on OD.
(2) The analysis of this material, at the OD indicated that it is consisted of S, FeS2, Fe2O3, SO2, FeS, and SiO2.
(3) Cl presence was detected under corrosion deposits at the ID.
(4) The major thickness reduction was due to corrosion at the ID.

E-7533 B: (1) At the OD morphology is typical of ammonium bi-sulfide corrosion, assisted by erosion phenomena
(2) At the ID corrosion morphology is similar to E-7533A but limited in extent.

From the above evidence the following conclusions can be drawn:
E-7533 A ID: Corrosion mechanism is under deposit corrosion due to Cl- in the cooling water.
E-7533 A OD: Corrosion proceeds uniformly with the formation of sulfides and oxides. In E-7533A thickness reduction is attributed mainly to the mechanism at the ID.
E-7533 B ID: Limited corrosion with a mechanism similar to that of E-7533A ID.
E-7533 B OD: The corrosion mechanism is ammonium bi-sulfide assisted by erosion. In E-7533B thickness reduction is attributed mainly to the mechanism at the OD.

3.7 Failure analysis investigation of the leaked tubes from the exchanger E-7207

Introduction: A refinery commissioned the Materials Laboratory of the University of Thessaly (LoM) to study the corrosion of heat exchangers' E-7207 tubes due to leakage during service. Laboratory tests involved chemical analysis, metallographic analysis, the use of stereo-optical microscopy, microhardness testing, the use of a scanning electron microscope (SEM), and X-ray diffraction (XRD).

Material selection: According to the refinery, the tube material is steel SA 179.

Operational conditions: From the shell side, the working environment is propane and from the tube side, the working medium is cooling water.

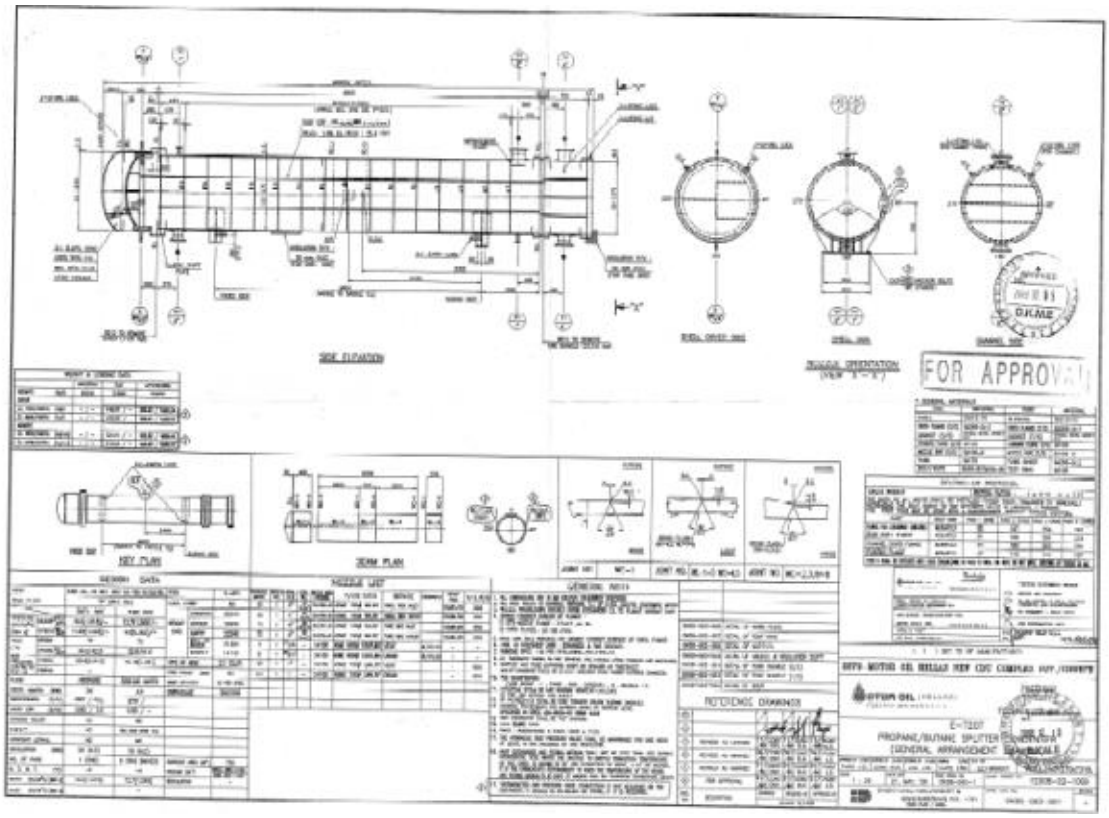

Table 3-10: Design data that are provided.

Parameter	Units	18/10/2013	21/10/2013	30/10/2013	6/11/2013	18/11/2013	25/11/2013	9/12/2013	17/12/2013	7/1/2014	20/1/2014	27/1/2014	2/2/2014	17/2/2014
		Cooling Tower Water												
pH		7,5	7,4	7,4	7,6	7,6	7,6	7,6	7,6	7,6	7,7	7,8	7,5	7,6
Specific cond.	µs/cm³	544	620	545	615	600	555	600	460	400	346	580	510	536
TH	ppm $CaCO_3$	85	120	75	81	90	90	88	70	50	55	85	82	75
P-Alkalinity	ppm $CaCO_3$	0	0	0	0	0	0	0	0	0	0	0	0	0
M-Alkalinity	ppm $CaCO_3$	21	20	20	27	26	22	22	14	22	25	22	20	20
Total - OPO4	ppm PO4-	9,45	9,5	13,8	8,5	12	11,4	8,9	7,9	8,7	9,5	10	11,2	7,85
Filtered- OPO4	ppm PO4-	8,45	8,2	9,6	6,8	8,2	11,2	7,5	6,8	7,9	6,4	5,6	8,75	6,45
T-Zn	ppm Zn+		-	-		-	-							
Total -Iron	ppm fe++	2,6	2,2	3,9	4,9	3,2	1,8	1,76	1,31	2,24	2,2	2,7	1,95	1,62
Iron - Soluble	ppm fe++	1,1	1,1	1,8	2,1	1,4	0,7	0,71	0,63	1,25	1,3	1,2	0,85	0,68
Copper	ppm Cu	-	-	-	-	-	-	-	-	-	-	-	-	-
Turbitity	NTU	-	-	-	-	-	-	-	-	-	-	-	-	-
Chlorides	ppm Cl-	48	55	75	69	75	60	70	52	50	52	80	45	74
Free Chlorine	ppm Cl2	0,2	0	0	0,7	0	0	0,1	0,1	0,2	0,1	0,2	0,1	0,1

Table 3-11: Concerning the cooling water on the tube side.

Chemical analysis (wt.%): Chemical analysis was performed on the tube material. The results are provided, and the requirements of the relevant specifications are also given. Chemical analysis showed that the Mn content is higher than the maximum specified limit.

	C	Si	Mn	P	S	Cr	Ni
E-7207	0.10	0.21	1.5	0.01	0.01	0.04	0.02
ASTM A179	0.06-0.18	-	0.27-0.63	0.035 max	0.035 max	-	-

Table 3-12: The results of chemical analysis.

Stereo–optical examination: Stereo–optical examination showed that the outer surface of the tubes is almost clear from corrosion phenomena. The inner surface of the tubes exhibited extensive corrosion phenomena associated with the formation of a thick layer of corrosion products, leading to failure. Deep pits were found within the corrosive layer. These pits evolved through tube thickness leading thus to perforation.

Metallography and microhardness measurements: Metallography and microhardness measurements showed that the microstructure of the steel consisted of ferrite and pearlite, as expected from the quality of the steel. Pitting started on the ID and progressed toward the OD at the expense of the tube thickness. Inside the pit corrosion products remained. The average microhardness was $107HV_{0.3.}$

SEM and EDX analysis: SEM and EDX analysis indicated high Cl presence, probably from the cooling water, ranging from 2.24-18.5wt%, at the interface region between the corrosion products and the steel, indicating hydrolysis mechanism and formation of HCl, while at the middle of the pit area, only Fe and O were identified indicating oxide formation.

EDX analysis: The X-ray diffraction analysis was carried out on the inner surface of the tube to identify the nature of the corrosion products found. Iron oxides were detected i.e., Fe_2O_3, FeO, Fe_3O_4.

Conclusions: The results presented above can be summarized as follows:
(1) The tubes failed because of pitting corrosion taking place at the inner surface of the tubes.
(2) SEM/EDX analysis showed Cl presence at the corrosion front, indicating hydrolysis mechanism and formation of HCl.
(3) The corrosion process takes place below the corrosion products, indicating an under-deposit corrosion mechanism due to Oxygen depletion.
These findings lead to the conclusion that the failure of the heat exchanger tubes is due to Cl pitting corrosion. Possibly this Cl is coming from the cooling water.

3.8 Failure analysis: tubes from R-3701 & E-3214 A

Introduction: A refinery commissioned the Materials Laboratory of the University of Thessaly (LoM) to study the corrosion of heat exchangers' E-3214 A and R-3701 tubes. Laboratory tests involved chemical analysis, metallographic analysis, the use of stereo-optical microscopy, microhardness testing, the use of a scanning electron microscope (SEM), and energy-dispersive X-ray analysis (EDX).

Material selection: Regarding R3701 the material of the tubes is the 70/30 Cupro Nickel (UNS C71500), which according to the Nelson diagram (Zone 7) is not suitable for this service.
Regarding E3214-A the material of the tubes is the CuZn20Al2 (ASTM B111).

Operational conditions: Regarding R3701 according to the refinery the tubes operated at: Temperature: 25-38°C, Pressure: 13.0 – 14.5kg/cm^2. The outer surface was exposed to HF with a small amount of Propane and oxygenate compounds, acetones, Butanes, and Alkylate all in liquid form. 90% of the liquid was HF, 0,5% humidity and the rest were Acid Soluble Oils (ASO). On the inner surface, there was a flow of seawater.
Regarding E3214-A according to the refinery the process side operated at Tin=41°C & Tout=32°C, pressure 1,5kg/cm^2-g with H/C (fuel gas, naphtha, LPG, H2S, etc.). On the inner surface, there was a flow of seawater.

Chemical Analysis (wt.%): Chemical analysis was performed for both R3701 and E3214-A.

	Cu	Ni	Fe	Mn	P	Zn	Pb	Sn	Si	Al
R3701	66,1	32,2	0,97	0,49	0,01	0,18	0,01	0,01	-	-
E3214-A	77,8	-	0,02	-	-	19,9	-	<0,01	0,04	2,2

Table 3-13: The results of chemical analysis.

Stereo-optical examination: Regarding R3701 stereo -stereo-optical examination indicated certain areas at the outer surface where complete perforation of the tubes happened. The openings had an oval shape either parallel or perpendicular to the main axis of the tubes. Corrosion products had accumulated on the outer surface in the vicinity of the "openings".
Regarding E3214-A stereo -optical examination indicated that the tubes were almost intact on their outer surface, while their inner surface had been covered by a black layer. Even though it was not possible to locate perforated areas, the investigation was focused on the deep isolated pits that were observed within the black layer

SEM/EDX analysis: Regarding R3701 SEM/EDX analysis showed that the corrosion products consisted mainly of oxides.
Regarding E3214-A SEM/EDX analysis S and Cl were detected, with compositions between 0,76-11,55% wt. for Sulfur and 1,42-3,78% for Chlorine.

Metallography: Regarding R3701 metallography demonstrated clearly that the failure of the tube is related to the environment of the outer surface. The corrosion phenomena evolved at the outer surface and dissolved the tube material up to the inner surface leading to local perforation, while there were areas unaffected by corrosion.
Regarding E3214-A metallography identified the corrosion as pitting corrosion at the inner surface. The corrosion front was located beneath the black layer and evolved towards the outer surface.

Conclusions: Regarding R3701 the material of the tubes is 70/30 CuproNickel (UNS C71500) which according to the Nelson diagram (Zone 7) shown in Fig. 34 is not suitable for this service.
Regarding E3214-A the detection of high quantities of Sulfur on the layer formed on the inner surface of the tubes suggests that due to some kind of leak process fluid entered the tube and was mixed with the seawater generating a highly corrosive environment. The material used is not suitable for this type of corrosive environment.

3.9 Root cause analysis on the corrosion of tubes from heat exchanger E-7512 B

Introduction: A refinery commissioned the Materials Laboratory of the University of Thessaly (LoM) to study the corrosion of a heat exchanger's E-7512 B tubes. Laboratory tests involved chemical analysis, metallographic analysis, the use of stereo-optical microscopy, microhardness testing, and the use of a scanning electron microscope (SEM). Stereo–optical examination found the outer surface (shell side) without significant corrosion problems from service conditions.

Material selection: According to the refinery, the tube material is carbon steel (CS).

Operational conditions: The relevant information concerning operational conditions which are given below:

Shell Side: H_2, T_{in}:95^oC, T_{out}: 30-35^oC, Tube side: H_2O T_{in}:25^oC, T_{out}: 30-35^oC, Skin Temperature: 65.1^oC, Water Velocity: 1.88m/sec, Heat flux: 40.5kW/m^{2}h, Tube material: CS, Thickness: 2.11 mm, D_{out}: 19.05mm, D_{in}: 14.83mm, L=4.88m. Water on tube side analysis gave: Fe++ increased to 2.51 ppm indicating corrosion of CS, Ryznar index 7.88> 6.0 indicating corrosion conditions.

Chemical Analysis: Chemical analysis was performed on the tube material.

	C	Si	Mn	P	S	Cu
E7512	0.09	0.19	0.41	0.01	0.01	0.17

Table 3-14: The results of chemical analysis.

Stereo–Optical examination: The outer surface (shell side) was found without significant corrosion problems from service conditions. On the contrary extensive deposits of corrosion products were found at the inner surface of the tubes. These deposits had locally a "blackish" and quite hard smooth surface typically associated with "brownish" porous layers underneath. Below these layers deposit corrosion (UDC) evolves dissolving the CS.

Metallography: The corrosion phenomenon is typical of under-deposit corrosion (UDC), which evolves at the inner surface beneath the accumulated corrosion products.

SEM/EDX analysis: According to the results, the corrosion products consist mainly of hydroxides or oxides of iron. The analyses indicate significant amounts of Cl at the corrosion front (pitting areas) along with corrosion products that are probably hydroxides or oxides of iron.

Conclusions: The results described above indicated the following issues:

(1) Presence of extensive deposits on the internal surface of the tubes: No presence of scale consisting of carbonates, phosphates, sulfates, or silicates of Ca or Mg. This is in line with velocity measurements (1.88m/s) in the normal zone. Deposits are hydroxides or oxides of iron as indicated by the EDX analysis. Severe corrosion below the oxide/hydroxide deposits. Metal dissolution has been detected from the increased Fe^{++} concentrations (2.51 ppm) in the cooling water analysis from MOH.

(2) Corrosion: EDX analysis indicated significant amounts of Cl in the corrosion front (pitting areas). The presence of Cl indicates an under-deposit corrosion (UDC) mechanism, similar to crevice corrosion, and is a result of a hydrolysis reaction, which originated from differential aeration cells formed between areas with deposits and the surrounding. In terms of working parameters: High skin temperature (65.1oC) accelerates the corrosion rate. Ryznar index is 7.88 on the corrosion rather than the scale formation side. Failure is the result of corrosion of carbon steel tubes. The corrosion mechanism is not related to scale formation but to under-deposit corrosion below iron oxide deposits. Skin temperature has played a role.

3.10 Failure analysis of tubes from E-1113

Introduction A refinery commissioned the Materials Laboratory of the University of Thessaly (LoM) to study the corrosion of a heat exchanger's E-1113 tubes. The flow in the tubes of the E1113 exchanger was mixed (liquid + gas). The gas phase contained H_2S. Laboratory tests involved metallographic analysis, the use of stereo-optical microscopy, microhardness testing, the use of a scanning electron microscope (SEM), Energy Dispersive X-ray analysis (EDX), and X-ray diffraction (XRD).

Operational conditions:

Case: Arabian Light		**AL**				
Stream Number				**Row**	**79**	**80**
Stream Phase		Stream Na	Stream Phase	1	Vapor	Mixed
Mass Rate	kg/h	Stream Na	Mass Rate	1	106742	106742
Vol. Flow Rate	m^3/h				23830.8	414.3
Temperature	°C	Stream Na	Temperature	1	128.8	45.0
Pressure	kg/cm^2	Stream Na	Pressure	1	3.43	3.13
Enthalpy	Mkcal/h	Stream Na	Enthalpy	1	22.110	2.816
Std.Liq.Sp.Gr.		Stream Na	Std. Liq. Sp. G	1	0.7276	0.7276
Std. API		Stream Na	Std. API	1	62.98	62.98
Act. Density	kg/m^3	Stream Na	Actual Density	1	4.6	264.1
UOP K factor		Stream Na	UOP K factor	1	11.98	11.98
Sulfur	PCT	Stream Na	Sulfur Content	1	0.0	0.0
Flash Point	°C	Stream Na	Flash Point Ter	1	25.8	25.8
Pour Point	°C	Stream Na	Pour Point Tem	1	-61.5	-61.5
Mass Rate	kg/h	Stream Na	Vapor Mass Ra	1	106742	818
MW		Stream Na	Vapor Molecula	1	63.38	40.60
Sp. Enthalpy	kcal/kg	Stream Na	Vapor Sp. Enth	1	202.063	116.723
CP	kcal/kg°C	Stream Na	Vapor CP	1	0.489	0.415
Act. Density	kg/m^3	Stream Na	Vapor Act. Den	1	4.592	3.223
Therm Cond	kcal/hm°C	Stream Na	Vapor Therm. C	1	0.0207	0.0199
Viscosity	cP	Stream Na	Vapor Viscosity	1	0.010	0.010
CP/CV Ratio		Stream Na	Vapor CP/CV R	1	1.079	1.145
Mass Rate	kg/h	Stream Na	Liquid Mass Ra	1	n/a	105924
Sp. Enthalpy	kcal/kg	Stream Na	Liquid Sp. Enth	1	n/a	25.034
CP	kcal/kg°C	Stream Na	Liquid CP	1	n/a	0.594
Act. Density	kg/m^3	Stream Na	Liquid Act. Den	1	n/a	704.7
Surf Tens	Dyne/cm	Stream Na	Liquid Surface	1	n/a	39.816
Therm Cond	kcal/hm°C	Stream Na	Liquid Therm. C	1	n/a	0.1105
Viscosity	cP	Stream Na	Liquid Viscosity	1	n/a	0.410
Liq Kin Visc	CST	Stream Na	Liquid Kinemati	1	n/a	0.497
H2O	wt %	Total Weig	H2O	1	12.04%	12.04%
H2S	wt %	Total Weig	H2S	1	0.48%	0.48%
METHANE	wt %	Total Weig	METHANE	1	0.15%	0.15%
ETHANE	wt %	Total Weig	ETHANE	1	0.00%	0.00%
PROPANE	wt %	Total Weig	PROPANE	1	0.31%	0.31%
IBUTANE	wt %	Total Weig	IBUTANE	1	0.62%	0.62%
BUTANE	wt %	Total Weig	BUTANE	1	4.79%	4.79%
IPENTANE	wt %	Total Weig	IPENTANE	1	3.70%	3.70%
PENTANE	wt %	Total Weig	PENTANE	1	7.23%	7.23%
C6 - NBP100	wt %	48	95	1	18.81%	18.81%
NBP100/150	wt %	105	145	1	36.68%	36.68%
NBP150/200	wt %	155	195	1	15.18%	15.18%
NBP200/250	wt %	205	245	1	0.01%	0.01%
NBP250/300	wt %	255	295	1	0.00%	0.00%
NBP300/370	wt %	305	365	1	0.00%	0.00%
NBP370+	wt %	375	906	1	0.00%	0.00%

Table 3-15: Operational conditions.

Stereo-optical microscopy: Stereo-optical microscopy showed that the inner surface was completely covered by a thick layer of corrosion products.

Metallographic analysis: According to metallographic analysis at the cross-section of the tube, a thick layer of corrosion products had accumulated on the inner surface. The corrosion front was below this layer dissolving progressively the tube material by forming wide pits. The microstructure of the material is typical ferritic-pearlite.

SEM/EDX analysis: SEM/EDX analysis was conducted on:

• The surface of the corrosion products and the results indicated the presence of Cl (up to 14%) alongside Fe, O, and S (up to 4,44%)
• The cross-section of the corrosion products and the results indicated the presence of Cl in the corrosion front and high S concentrations in the outer layer of the corrosion products.

XRD analysis: The XRD analysis, conducted on the corrosion products collected from the inner surface indicated the presence of several iron sulfides (FeS, $Fe_{1-x}S$, Fe_3S_4, Fe_9S_{11}) in addition to small amounts of Fe_2O_3.

Conclusions: According to observations of the MOH inspection department, the tubes suffered severe erosion in the tube entrance. This manifests a high flow velocity and, therefore, the type of mixed flow can be classified as turbulent. The presence of sulfides in the corrosion products (XRD analysis) indicates a low-temperature corrosion mechanism by dissolved H_2S. The thickness of the sulfide layers is large. Under these conditions (large thickness and turbulent flow) the sulfides are fragile and are removed by the flow. The remaining sulfides act as cathodes leading to the anodic dissolution of the steel, as evidenced by the cross-sections of the metallographic investigation. The presence of Cl in the corrosion front (EDX analysis) indicated the possible presence of HCl (in addition to H_2S), dissolved in the liquid. HCl could form from the hydrolysis of salts. Then the HCl causes under-deposit corrosion and acts synergistically with H_2S. The corrosion can be classified as low-temperature corrosion by dissolved H_2S and HCl.

3.11 Failure analysis of tubes from exchanger E-7502B

Introduction: A refinery commissioned the Materials Laboratory of the University of Thessaly (LoM) to study the corrosion of the heat exchanger's E-7502 B tubes. The tubes exhibited corrosion phenomena resulting in local pitting on several areas of the inner surface. Laboratory tests involved chemical analysis, metallographic analysis, the use of stereo-optical microscopy, microhardness testing, the use of a scanning electron microscope (SEM), Energy Dispersive X-ray analysis (EDX), and X-ray diffraction (XRD).

Material selection: According to the refinery, the tube material was austenitic stainless steel 321.

Operational conditions: •Medium: H_2+H_2S+H+H_2O+NH_3 and Temp: In 280^oC/ Out:190^oC

Chemical Analysis (wt.%): Chemical analysis was performed on the tube material.

C	Si	Mn	P	S	Cr	Mo	Ni	Nb	Ti	V	Cu	Co
0.05	0.46	1.91	0.036	<0.001	17.29	0.25	10.48	0.01	0.31	0.07	0.25	0.09

Table 3-16: The results of chemical analysis.

Stereo-optical examination: The results from the stereo-optical examination showed that half part of the inner surface was covered by "reddish" deposits. Deep pits had been formed in between these deposits whilst the same phenomena occurred at some areas of the inner surface where the "corrosion deposits" seem to be depleted by the washing treatment. The opposite side of the inner surface appeared clean without corrosion phenomena.

Metallography: According to metallography several pits were formed under the corrosion deposits at the inner surface of the tube and evolved towards the outer surface.

SEM/EDX analysis: SEM/EDX analysis was carried out on the inner surface of the tube, where the reddish corrosion products accumulated and pitting corrosion evolved. The deposits contain significant amounts of Sulfur, however, in the pitting areas, the Sulfur concentration is lower than at the rest of the surface. Cl had been detected in various amounts (0.02-0.87 %) in pit regions.

X-ray diffraction analysis: X-ray diffraction analysis was conducted on the deposits accumulated at the inner surface of the tube. The austenite phase of the SS 321 was identified as expected from the material. The deposits consist of Iron sulfide (FeS), Iron Oxide (Fe_2O_3), and ammonium bisulfite (NH_4SH).

Conclusions: The above results can be summarized as follows:

(1) Corrosion can be regarded as pitting corrosion taking place under deposits.

(2) Deposits on the tube surface are rich in sulfur. Ammonium bisulfide (NH4HS) has been detected by XRD.

(3) Sulfur is abundant on the alloy surface but much lower sulfur exists in the pitting regions (EDX)

(4) Cl has been detected in various amounts in pit regions (EDX)

According to MOH inspection data, the problem has been more severe between U-turns in the bundle, where fluid flow conditions favor deposit formation.

3.12 Overhead crude heat exchanger E-1103A tube failure analysis

Introduction: A refinery commissioned the Materials Laboratory of the University of Thessaly (LoM) to study the corrosion of heat exchangers' E-1103 A tubes of the Crude Distillation Unit (CDU). The exchanger exhibited leaks in the tubes after 10 months of operation. Laboratory tests involved metallographic analysis, the use of stereo-optical microscopy, the use of scanning electron microscope (SEM), Energy Dispersive X-ray analysis (EDX), and X-ray diffraction (XRD).

Material selection: The material of the tube is duplex stainless steel 2707 (UNS: S32707/ EN Number: 1.4658).

Stereo-Optical Examination: Stereo-optical examination indicated that the external surface of the tube was covered with deposits. The surface below the deposits revealed extensive pitting corrosion. These preliminary results showed a possible under-deposit corrosion mechanism.

Metallography: According to metallography specimens exhibited multiple pitting and the corrosion front. The corrosion front indicated the preferential corrosion of the ferrite phase.

EDX analysis: SEM/EDX analyses were conducted on the "reddish" side of the deposits (outer side) and the "blackish" side of the deposits (tube side, in contact with tube). The results of the EDX analysis indicated, in addition to the expected alloying elements, the presence of S and Cl in significant quantities. However, S appeared exactly on the corrosion front, while Cl appeared in the successive corrosion layers. This manifests the presence of possibly FeS film, which is broken by Cl due to the corrosion surface.

XRD analysis: XRD analysis was carried out to confirm the presence of FeS as well as the presence of salts in the deposits. X-ray diffraction was performed on the deposits on both the black side (in contact with
the tube surface) and the red side (free surface of deposits). The results are:
Black side (in contact with tube): Fe_2O_3, Fe_3O_4, Fe_3S_4, FeS, FeS_2, NH_4Cl, $NH_4Cl(NH_3)_3$, $N_2H_6Cl_2$.
Red side (free surface of deposits): Fe_3S_4, FeS, Fe_xO, Fe_3O_4, Fe_2O_3, NH_4Cl, $N_2H_6Cl_2$, N_2H_5Cl
It is important to note the presence of several amine salts and FeS.

Conclusions: The results of the current investigation indicated extensive under-deposit corrosion with multiple pitting areas. Deposits contain oxides, sulfides, and chlorides. The

chlorides, in particular, are NH_4Cl, $N_2H_6Cl_2$, and $NH4Cl(NH_3)_3$, are amine chlorides arising from the main neutralizer amine used (MEA) or may contain tramp amines from cycling in the system. The results so far indicate the breakdown of the protective FeS film by Cl, as S was detected at the corrosion front, while Cl was detected at the succeeding corrosion layers. This film breakdown leads to rapid localized corrosion in the form of pitting corrosion. However, the Cl effect is coming from the amine salts deposited during the operation of the exchanger. The conditions (salt point) were such that allowed the deposition of amine salts and the operation of an under-deposit corrosion mechanism. The observed corrosion of the E1103A tubes is an under-deposit corrosion mechanism that is activated by the deposition of amine salts on the tube surface. The under-deposit corrosion led to the breakdown of FeS passive films, leading to rapid localized corrosion in the form of pitting.

3.13 Failure analysis of tubes from heat exchanger E-3711

Introduction: A refinery commissioned the Materials Laboratory of the University of Thessaly (LoM) to study the corrosion of heat exchangers' E-3711 tubes. The tubes experienced clogging and thinning during service. Laboratory tests involved chemical analysis, metallographic analysis, the use of stereo-optical microscopy, the use of scanning electron microscope (SEM), Energy Dispersive X-ray analysis (EDX), and X-ray diffraction (XRD).

Material selection: According to the refinery, the tube material is the ASTM A179 steel seamless cold-drawn low-carbon steel.

Operational conditions: The OD is 19.05mm and the thickness is 2.1mm. The process in the tube side is HC + dissolved HF, T_{in}= 48oC, T_{out}= 69ºC, and P=13.34 Kg/cm^2. At the shell side, the relevant values are HC+ trace HF (gasoline) T_{in}=189ºC, T_{out}=79ºC, and P=10.25 Kg/cm^2. MOH provided also daily process data, taken during the last year of operation. The data indicated that the max temperature on the tube side was 65.2ºC.

Chemical analysis (wt.%): Chemical analysis was carried out on the tube material. The results are provided, where the requirements of the relevant specification for ASTM A179 are also given. The last column of the table indicates the number of residual elements (RE) contained in the steel.

	C	Si	Mn	P	S	Cr	Ni	Cu	Al	RE (*)
TUBE 3711	0.07	0.24	0.50	0.01	0.01	0.11	0.10	0.16	0.03	0.37
ASTM A179	0.06-0.18	-	0.17-0.63	0.035 max	0.035 max	-	-	-	-	-

(*)RE= Cr+Ni+Cu

Table 3-17: The results of chemical analysis.

Stereo-Optical Examination: The stereo-optical examination was performed on the inner and outer surfaces of the tube. The outer surface of the tube appeared without evidence of corrosion, while at the inner surface, a thick layer of corrosion products has been accumulated. These products are quite well adhered to the inner surface of the tube and appear to have a brownish color on their surface, while the color changed to blackish on their surface in contact with the steel. Their thickness is similar to the thickness of the steel. There are indications of local deterioration of the layer of corrosion that leads to exposure of the underlying steel to the process environment, accelerating the corrosion phenomena. The steel underneath this layer exhibits a characteristic "silver" appearance which coexists with local corrosion products still adhered to the inner surface of the steel. The remaining thickness was measured between 1.9 and 1.5mm.

Metallography: The microstructure of the steel consists of ferrite and perlite. At the inner surface the corrosion front forms wide undercuts below the ID.

SEM/EDX analysis: SEM/EDX analysis was conducted at the inner surface of the tube and on the surface of the corrosion products. The results indicated that the corrosion products consist mainly of F and Fe. Smaller quantities of O and C were also detected.

X-ray Diffraction: The removed corrosion products were further analyzed by XRD. The blackish side - in conduct with the inner surface of the tube- consists of FeF_2, while the brownish side beside the FeF_2 contains also iron oxides (Fe_2O_3, Fe_3O_4).

Conclusions: The corrosion proceeds from the tube side. The presence of iron fluoride deposits points to Hydrofluoric Acid Corrosion, according to API 571. The corrosion is mostly general corrosion leading to thinning of the tube wall. The clogging observed in several tubes is caused by iron fluoride corrosion products.

Several factors accelerate HF corrosion:

(1) Residual elements (RE) in steel. Cr, Ni, and Cu were detected with total RE=0.37, which is above the 0.2% limit referred to in API 571. These impurities contribute to accelerated corrosion.

(2) Sulfur compounds in the process stream also accelerate HF corrosion. The EDX analysis indicated that there is no Sulfur in the corrosion products.
(3) Water in the process stream promotes HF dilution and HF corrosion of carbon steel. In addition, it can destabilize the iron fluoride scale and convert it from protective to non-protective. The presence of water promotes the formation of acid-soluble oils (ASO), which are soluble in HF and accelerate corrosion. The water entry should be checked and minimized by the refinery.
(4) Dissolved oxygen accelerates the corrosion rate by HF. Oxygen concentrations should be also checked and minimized by the refinery.
(5) Temperature: The records indicate that the max temperature on the tube side remained below the API 571 66ºC limit (max T_{out} was 65.2ºC) for the reference period.

3.14 Failure analysis of tubes from heat exchanger E-3707

Introduction: A refinery commissioned the Materials Laboratory of the University of Thessaly (LoM) to study the corrosion of heat exchangers' E-3707 tubes. The tubes experienced clogging and thinning during service. Laboratory tests involved chemical analysis, metallographic analysis, the use of stereo-optical microscopy, the use of scanning electron microscope (SEM), and Energy Dispersive X-ray analysis (EDX).

Material selection: According to the refinery, the tube material is the ASTM B111 (Cu-30Ni alloy, 0.4-1.0 Fe, 1.0Mn, 1.0Zn).

Operational conditions: The OD is 19.05mm and the thickness is 2.1mm. The process in the tube side is seawater, Td= 93oC (design), Top= 29.5-38oC (operating), and P=11 Kg/cm^2. At the shell side, the relevant values are HC+ trace HF, Tin=189oC, T_d=91ºC, T_{op}=63-68oC, and P=23.8 Kg/cm^2. MOH provided also the tube testing report (eddy current) issued by MISTRAS HELLAS A.B.E.E.

Chemical Analysis (wt.%): Chemical analysis was performed on the tube material. The results are provided, and the requirements of the relevant specifications are also given.

	Mn	Fe	Ni	Cu	Pb	Zn
TUBE 3707	0.81	0,83	30	rem	-	-
ASTM B111 UNS C71500	1.0 max	0.40-1.00	29.00-33.00	rem	0.05 max	1.0 max

Table 3-18: The results of chemical analysis.

Stereo-Optical Examination: The stereo-optical examination was performed on the inner and outer surfaces of the tube. The outer surface of the tube appeared without evidence of corrosion/erosion while at the inner surface corrosion attack was in the form of elliptical craters characteristic of an erosion mechanism. The craters have been formed mainly at the one edge of the provided tube segment. The pattern of the craters is oriented parallel to the tube's main axis.

Metallography: The microstructure of the material- typical of the 70/30 alloy consists of the alpha phase. At the inner surface, the corrosion front is in the form of craters below the ID.
SEM/EDX analysis: SEM/EDX analysis was conducted at the inner surface of the tube, where the erosion craters have been formed. The results indicated the presence of sulfur (S) in the interior of the craters.

Conclusions: Cu-30Ni alloys have been extensively used in heat exchangers with tube-side sea water with generally good results. However, corrosion problems can take place for various reasons, the most important are outlined below:
(1) Suspended solids in seawater: They cause erosion-corrosion, depending on velocity, solids content, and particle size.
(2) Pollutants: The main pollutants affecting the corrosion of Cu-30Ni are sulfide and ammonia. They can affect corrosion even at very low concentrations. It has been reported that as little as 0.01mg/lt of sulfide can cause corrosion problems in Cu-Ni alloys. These problems are most common in land-based heat exchangers.
(3) Antifouling additions: Usually chlorine/hypochlorite are added as antifouling agents. Sometimes they can lead to increased corrosion rates.
(4) Velocity: High local velocity or turbulence can increase erosion rates. The max velocity limit set by the Copper Development Association for heat exchanger tubing is 2.5-3.5m/s.
(5) Quality of tubing material: It has been reported that the presence of carbon film on the ID of the tubes, from the manufacturing process, can accelerate the corrosion process in seawater.
The results presented above indicated that the corrosion attack was in the form of elliptical craters characteristic of an erosion process. In addition, the EDX analysis indicated the presence of sulfur (S) in the interior of the crates. These observations lead to the conclusion that the thinning of the tubes was due to an erosion-corrosion mechanism by seawater polluted with sulfides.

3.15 Failure analysis of tubes from heat exchanger E-3713

Introduction: A refinery commissioned the Materials Laboratory of the University of Thessaly (LoM) to study the corrosion of heat exchangers' E-3713 tubes. The tubes failed due to corrosion-erosion. Laboratory tests involved chemical analysis, metallographic analysis, the use of stereo-optical microscopy, the use of scanning electron microscope (SEM), and Energy Dispersive X-ray analysis (EDX).

Material selection: According to the refinery, the tube material is the ASTM B111 (Cu-30Ni alloy, 0.4-1.0 Fe, 1.0Mn, 1.0Zn).

Operational conditions: The OD is 19.05mm and the thickness is 2.1mm. The process in the tube side is seawater, T_{in}= 27^{o}C, p=1.5-2 Kg/cm2, Tout= 40^{o}C, p=0.5-1 Kg/cm^2. At the shell side, the relevant values are C4s + trace HF, T_{in}=82^{o}C, p=8.7 Kg/cm^2, T_{out}=40^{o}C, and P=8.4 Kg/cm^2. MOH provided also the tube testing report (eddy current) issued by MISTRAS HELLAS A.B.E.E.

Chemical Analysis (wt.%): Chemical analysis was performed on the tube material. The results are provided, and the requirements of the relevant specifications are also given.

	Mn	Fe	Ni	Cu	Pb	Zn
TUBE 3713	0.66	0.85	30.8	rem	-	-
ASTM B111 UNS C71500	1.0 max	0.40- 1.00	29.00- 33.00		0.05 max	1.0 max

Table 3-19: The results of chemical analysis.

Stereo-Optical Examination: The stereo-optical examination was performed on the inner and outer surfaces of the tube. The outer surface of the tube appeared without evidence of corrosion/erosion while at the inner surface corrosion attack was in the form of elliptical deep craters characteristic of an erosion mechanism. The pattern of the craters is oriented parallel to the tube's main axis.

Metallography: The microstructure of the material- typical of the 70/30 alloy consists of the alpha phase. At the inner surface, the corrosion front is in the form of craters below the ID.

SEM/EDX analysis: SEM/EDX analysis was conducted at the inner surface of the tube, where the erosion craters have been formed. The results indicated the presence of sulfur (S) in the interior of the craters.

Conclusions: The observed thinning of the heat exchanger tubes is attributed to the erosion-corrosion mechanism. Sulfide pollution in seawater has contributed to the corrosion process.

3.16 Failure analysis of tubes from heat exchanger E-7120

Introduction: A refinery commissioned the Materials Laboratory of the University of Thessaly (LoM) to study the corrosion of heat exchangers' E-7120 tubes with emphasis on the shell side. The tubes experienced thinning and local perforation which led to bundle replacement in 9 months (1/09/17- 02/05/18). The corrosion was more intense in the center of the tube bundle. Laboratory tests involved chemical analysis, metallographic analysis, the use of stereo-optical microscopy, the use of scanning electron microscope (SEM), Energy Dispersive X-ray analysis (EDX), and Energy Dispersive X-ray analysis (EDX).

Operational conditions: On the tube side, there was cooling water.
On the shell side, there was naphtha, with T_{in} varying between 35 and 58^{o}C and Tout between 26 and 41^{o}C. Other process data were given: Pressure 0.7 to 1.0 Kg/cm^2, TAN= 0,022 mg KOH/g, Water phase: 10%, Chlorine in organic phase = 0,9 ppm, Chlorine in water phase= 3,0 ppm, H2S in organic phase: 55 ppm, H2S in water: 27 ppm.

Chemical Analysis (wt.%): Chemical analysis was performed on the tube material.

	C	Si	Mn	P	S	Cr	Ni	Cu	Al
TUBES 7120	0.10	0.24	0.51	0.02	0.01	0.03	0.02	0.03	<0.01

Table 3-20: The results of chemical analysis.

Stereo-Optical Examination: The stereo-optical examination was performed both on the outer and the inner surfaces of the tubes. The surface of the tubes (OS) was covered by "reddish" corrosion products loosely adhered to the tube. These products were collected and analyzed by XRD. Corrosion products were also accumulated at the inner surface (IS). The corrosion phenomena led to the thinning of the tube's walls both from the inner and the outer sides resulting in local perforation.

Metallography: The microstructure consists of ferrite and pearlite. Corrosion phenomena were observed on both the inner and the outer surfaces of the tube. The formation of wide pits, where the corrosion products were accumulated, characterizes the inner surface, while the corrosion morphology at the shell side is characterized as uniform corrosion, leading to uniform thinning of the tube wall from the shell side.

SEM/EDX analysis: SEM/EDX analysis was conducted on the corrosion products observed in the metallographic analysis. The results indicate that the corrosion products consist mainly of O and Fe. Considerable concentrations of Cl (up to 4.66 wt.%) and S (up to 3.23 wt.%) were locally detected on both sides with higher concentrations at the IS.

X-ray Diffraction: The collected corrosion products from the outer surface of the tubes were further analyzed by XRD. The corrosion products consist of Iron Oxides (Fe_2O_3, Fe_3O_4, FeOOH) and sulfides (FeS).

Conclusions: The data presented above, regarding the corrosion of the shell side of E-7120, can be summarized as follows:

(1) The corrosion proceeds from both sides, the shell side and tube side

(2) The corrosion is more intense in the center of the tube bundle, as shown by the photos provided by MOH.

(3) The surface of the tubes (OD) was covered with corrosion products. The XRD analysis of the corrosion products indicated the presence of iron oxides and sulfides.

(4) Temperature at the shell side is too low for naphthenic acid corrosion.

(5) The EDX analysis performed on metallographic specimens indicated the presence of S and Cl at the corrosion front.

(6) The EDX results are consistent with the presence of H2S (27ppm) and Chlorine (3ppm) in the water phase (10% of the total stream).

(7) The results above, indicate that the corrosion mechanism is attributed to acid corrosion (anodic dissolution) of carbon steel, by sulfuric and/or hydrochloric acid, which formed at the shell side, due to H2S and water in the naphtha. Stagnant conditions at the center of the tube bundle might have contributed to the corrosion by increasing the local concentrations.

(8) The corrosion morphology at the shell side is characterized as uniform corrosion, leading to uniform thinning of the tube wall from the shell side.

The corrosion at the shell side of E-7120 is due to uniform acidic corrosion due to the formation of sulfuric and/or hydrochloric acid in the process stream. Stagnant conditions might have contributed to the corrosion. The corrosion front is uniform leading to uniform thinning of the tube wall. The corrosion at the tube side, due to cooling water, appears more severe and localized. Perforation of the tubes at the center of the bundle is due to the combination of both types of corrosion, tube side, and shell side.

3.17 Root cause analysis of internal pitting in the tube from exchanger 100-E-03c

Introduction: A refinery commissioned the Materials Laboratory of the University of Thessaly (LoM) to study the corrosion of heat exchangers' 100-E-03c tubes analysis concerning pitting detected at the tube side. Laboratory tests involved chemical analysis, metallographic analysis, the use of stereo-optical microscopy, the use of scanning electron microscope (SEM), and Energy Dispersive X-ray analysis (EDX).

Material selection: According to the refinery, the tube material is the SA-213 TP321 stainless steel.

Operational conditions: The design pressure was 48kg/cm^2 and the design temperature was 425^{o}C. The process stream involved H_2O (0,15 mol%) + H_2 (52,85 mol%) + H_2S (3,56 mol%) + HC (43,44 mol%).

Chemical Analysis (wt.%): Chemical analysis was performed on the tube material. The results are provided, and the relevant specification requirements are also given.

	C	N	Si	Mn	P	S	Cr	Mo	Ni	Cu	Ti
Tube	0.03	0.04	0.49	1.70	0.04	<0.01	17.4	0.22	9.7	0.99	0.26
TP 321 ASTM A213	0.08 max	-	1.0 max	2.00 max	0.045 max	0.03 max	17.0-19.0	-	9.0-12.0	-	0.25 -0.46 (*)

(*) taking into account the uncertainty in measurements of C, N

Table 3-21: The results of the chemical analysis

Stereo-Optical Examination: Besides the main finding concerning the deep pit some smaller/shallower pits were also observed around the same area. All pits exhibited similar morphology and were grown within a thin layer of corrosion products, well-adhered on the tube's inner surface.

Metallography: The pit had already penetrated ~ 1/3 of the tube thickness, and within its cavity, several corrosion products were accumulated. At the corrosion front a "gray" almost "compact" zone was observed, exhibiting similar characteristics with the layer of the corrosion products formed at the inner surface outside the pits. Behind the corrosion front - the morphology appeared "porous" both inside and outside the pitting.

SEM/EDX analysis: SEM/EDX analysis was carried out on the inner surface at the vicinity of the pitting and on selected areas of the metallographic specimen. At the inner surface, high S concentrations were detected (up to 41.01 wt.%) associated with significant Cl presence (up to 1.42 wt.%) and low Cr and Ni concentrations. Similar results were found from the analyses performed at the cross-section of the pitting, where Cl (up to 1.32 wt.%) and S (up to 53.76 wt.%) were detected at the corrosion front within the pit area. It is worth noting that the thin layer of the corrosion products contains also significant amounts of S and Cl.

Conclusions: The results from the laboratory analyses can be summarized as follows:

(1) There were several pits at the inner surface of the tube examined, the deeper had propagated almost at 1/3 of the tube thickness.
(2) Corrosion products had accumulated at the inner surface of the tube and inside the pits-mainly at the corrosion front. The EDX analysis revealed high local concentrations of S and Cl.
(3) The presence of Cl indicates a pitting corrosion mechanism, due to Chlorides in the stream.
The findings point out a pitting corrosion mechanism due to Chlorides in the stream, which caused the local breakdown of the passive protective film.

3.18 Failure analysis of corrosion of tubes from cooler Em-1113

Introduction: A refinery commissioned the Materials Laboratory of the University of Thessaly (LoM) and the Shipbuilding Technology Laboratory-National Technical University of Athens (STL), to study the corrosion of air cooler Em-1113 tubes. Laboratory tests involved chemical analysis, metallographic analysis, the use of stereo-optical microscopy, the use of scanning electron microscope (SEM), and Energy Dispersive X-ray analysis (EDX).

Material selection: According to the refinery, the tube material is carbon steel.

Operational conditions: According to the data supplied by the refinery, the process stream is naphtha (top of distillation column) containing H2S and possibly chloride and nitrate salts.

Chemical Analysis (wt.%): Chemical analysis was performed on the tube material.

	C	Si	Mn	P	S	Cr	Mo	Ni	Cu	Al
Tube	0.08	0.18	0.45	0.009	0.011	0.11	0.05	0.09	0.19	0.027

Table 3-22: The results of chemical analysis.

Stereo-Optical Microscopy: It was found that the surface was covered by corrosion products.

Metallography: Wide and shallow corrosion pits at the ID were detected with an accumulation of corrosion products.

SEM/EDX analysis: SEM/EDX analysis was performed at the inner surface of the tubes. Corrosion products consisted mainly of Fe and O. Limited presence of S was detected.

XRD analysis: The scale carefully collected from the inside tube surface was further analyzed by XRD. The scale consisted of iron sulfate $FeSO_4$, iron oxide Fe_2O_3, and iron sulfide FeS_2 (marcasite).

Conclusions: The results presented above can be summarized as follows:

(1) Metallographic sections indicated mild corrosion with wide and shallow pits and limited thickness reduction.

(2) The SEM/EDX analysis deposits at the inside surface indicated Fe, O, and a limited concentration of S.

(3) The XRD analysis of scale from the inside surface indicated the formation of $FeSO_4$, FeS_2, and Fe_2O_3.

The above observations point to the mechanism of H_2S corrosion with the formation of oxides and iron sulfide FeS_2. The corrosion attack is mild with limited thickness reduction.

3.19 Overview of the cases

The case studies presented and further analyzed are summarized in Table 3-23. They emphasize the observation that heat exchanger failures are a result of combined operational issues, design flaws, and material deficiencies. The majority of these cases failed due to pitting corrosion, with a smaller percentage failing because of erosion or erosion-corrosion and individual cases have general corrosion, H_2S, or acid corrosion as their failure mode.

Laboratory tests involved visual inspection using a stereo-optical microscope, metallographic analyses, micro sclerometers, the use of a scanning electron microscope (SEM), X-ray diffraction (XRD), and Energy Dispersive X-Ray Analysis (EDX).

Given the material selected for each case with its chemical analysis, the operational conditions, and the results of each laboratory test we can assume with great precision not only the failure mechanism but also the reasons that led to it, to take the proper countermeasures for each case.

In the majority of these case studies we observe Chlorine (Cl) presence at the corrosion front, indicating hydrolysis mechanism and formation of HCl. The presence of Cl is probably from the cooling water that is used as the tube side fluid in most cases. In case naphtha is used as the shell side fluid, the presence of H_2S in the stream of naphtha causes local corrosion with the formation of pyrrhotite FeS1.15. In general Sulfur appears to be a common element in deposits. Finally, in most of the cases thickness reduction is attributed mainly to the failure mechanisms.

Study	Study number	Heat-exchanger number	Shell side fluid	Tube side fluid	Tube material	Failure Mode
Failure study of a. Sea exchanger tube and b. Flexible EADC transport pipeline					a. ASTM B111-687 b. Stainless steel	a. Erosion-corrosion, b. Pitting corrosion
Corrosion study of E-1103B exchanger tubes		E-1103B	Naphtha	Well fluids (Methane, hydrogen, sulfide, water)	SANICRO 28	Pitting corrosion (Barnacle-type corrosion)
Failure study of E7114 exchanger tube		E7114	Crude	LGO	ASTM A335 P5	Erosion and pitting corrosion
Study of causes of corrosion of E-7528 exchanger tubes		E-7528	H_2+H_2S+H+H_2O+NH_3	Cooling water	SA 210-A1	ID: Pitting corrosion (Under-deposit corrosion) , OD: Ammonium bisulfite corrosion
Evaluation of the cleaning of the internal surface of the E-3310 exchanger		E-3310			Stainless steel 410	
Failure analysis investigation of tubes from the heat exchangers E-7533 A & B	Rep. 0151/2013	E-7533 A & B	Heavier HC+ MDEA+ Methane+ Propane +Butane + Ibutane+ Ethane+ H_2 + H_2S + H_2O+ NH_3	Cooling water	SA 210 A-1	A. Exfoliation-type corrosion, Under-deposit corrosion, B. Ammonium bisulfite corrosion + Erosion
Failure analysis investigation of the leaked tubes from the exchanger E-7207	Rep. 0173/2014	E7207	Propane	Cooling water	ASTM A179	Pitting corrosion
Failure analysis: tubes from R-3701 & E-3214 A	Rep. 225/2016	R3701 & E3214-A	R3701: HF with a small amount of Propane and oxygenate compounds, acetones, Butanes, and Alkylate all in liquid form, E3214-A: fuel gas, naphtha, LPG, H2S, etc	R3701: Seawater, E3214-A: Seawater	R3701: CuproNickel (UNS C71500), E3214-A: ASTM B111	R3701: Pitting corrosion E3214-A: Pitting corrosion
exchanger E-7512 B	Rep. 233/2017	E-7512 B	H2	Cooling water	Carbon steel	Pitting corrosion (Under-deposit corrosion)
Failure analysis of tubes from E-1113	Rep. 242/2017	E-1113		mixed (liquid + gas). The gas phase contains H2S		Low-temperature corrosion by dissolved H2S and HCl
Failure analysis of tubes from exchanger E-7502B	Rep. 252/2017	E-7502B	H2+H2S+H+H2O+NH3		Stainless steel 321	Pitting corrosion
					Stainless steel	

Root cause analysis on the corrosion of tubes from heat exchanger E-7512 B	Rep. 233/2017	E-7512 B	H2	Cooling water mixed (liquid + gas). The gas phase contains H2S	Carbon steel	Pitting corrosion (Under-deposit corrosion)
Failure analysis of tubes from E-1113	Rep. 242/2017	E-1113				Low-temperature corrosion by dissolved H2S and HCl
Failure analysis of tubes from exchanger E-7502B	Rep. 252/2017	E-7502B	H2+H2S+H+H2O+NH3		Stainless steel 321	Pitting corrosion
Overhead crude heat exchanger E-1103A tube failure analysis	Rep. 262/2017	E-1103A			Stainless steel 2707 (UNS: S32707/ EN Number: 1.4658)	Pitting corrosion (Under-deposit corrosion)
Failure analysis of tubes from heat exchanger E-3711	Rep. 269/2018	E-3711	HC+ trace HF (gasoline)	HC + dissolved HF	ASTM A179	General corrosion
Failure analysis of tubes from heat exchanger E-3707	Rep. 271/2018	E-3707	HC+ trace HF	Seawater	ASTM B111	Erosion-corrosion
Failure analysis of tubes from heat exchanger E-3713	Rep. 272/2018	E-3713	C4s + trace HF	Seawater	ASTM B111	Erosion-corrosion
Failure analysis of tubes from heat exchanger E-7120	Rep. 276/2018	E-7120	Naphtha	Cooling water		Acid corrosion
Root cause analysis of internal pitting in the tube from exchanger 100-E-03c	Rep. 279/2018	100-E-03c			ASTM A213 TP321	Pitting corrosion
Failure analysis of corrosion of tubes from cooler Em-1113	Rep. 10/2022	Em-1113	Naphtha		Carbon steel	H2S corrosion

Table 3-23: Summarized table of case studies.

4. GUIDELINES

4.1 Design considerations

4.1.1 Material selection and compatibility

A proper material selection in combination with heat treatment would help avoid many issues. The right material could be selected based on the following process:

i. Defining the requirements of the heat exchanger,
ii. Creating a strategy for assessing candidate materials,
iii. Identifying them,
iv. Evaluating them and,
v. Selecting the optimum.

Regarding step number one parameters such as the nature of the fluids on both the shell side and tube side, the flow rate, the pressure, the temperature, and other conditions like startup and shutdown conditions, upset conditions, and special conditions such as product purity requirements, hazardous effects of intermixing of fluids, radioactivity, and maintenance should be taken into consideration. Welding is also an important parameter.

The strategy that is about to be established needs to consider and combine factors such as cost -the use of not-so-expensive materials- and reliability -the most reliable material regardless of the cost.

Considerations influencing material selection include:

I. Physical properties
    i. High heat transfer coefficient (requiring high thermal conductivity for tube material),
    ii. Thermal expansion coefficient to be low and as compatible as possible with those of the materials used for tube sheet, tube support, and shell to provide resistance to thermal cycling.

II. Mechanical properties
    i. Good tensile and creep properties (High creep rupture strength at the highest temperature of operation and adequate creep ductility to accommodate localized strain at notches are important).
    ii. Good fatigue, corrosion fatigue, and creep-fatigue behavior.
    iii. High fracture toughness and impact strength to avoid fast fracture.

III. Corrosion resistance

i. Low corrosion rate to minimize the corrosion allowance (and also radioactivity control in heat exchangers for the nuclear industry),
ii. Resistance to corrosion from off-normal chemistry resulting from a leak in the upstream heat exchanger or failure in the chemistry control,
iii. Tolerance to chemistry resulting from a mix-up of shell and tube fluids.

The manufacturing route is also important involving joining of the tube to tube sheet by welding, rolling, or both, or bending of tubes, forming of shell geometry and welding of shell plates and shell to the nozzle, and the heat treatments associated with the welding steps.

Recommended materials for specific occasions for nuclear power plant heat exchangers:

i. *Pressurized Water Reactor:* Mill-annealed Inconel 600 has displayed the most failures, so it has been replaced with alloy 600 with thermal treatment, alloy 690 annealed or with thermal treatment, and alloy 800. A comparison of these three is presented in the table below. Also, alloy 690 TT and 9Cr-lMo-V- Nb-N (91 Grade) or 9Cr-1.7W-0.5Mo-V-Nb-N are good choices. Cr-Mo alloys provide higher flexibility due to their high thermal conductivity and low expansion coefficient, than austenitic steel.

CHARACTERISTICS	ALLOY 800	ALLOY 600		ALLOY 690	
		annealed	specially heat treated	annealed	specially heat treated
CHEMISTRY					
. Chromium %	**	*		***	
. Nickel %	*	***		**	
. Desirable Cobalt %	$\geq$.10 OK	$\geq$.10 not always sufficient - $\geq$05		$\geq$10	OK
. Insensitivity of mechanical corrosion properties to variations in heat to heat analyses or thermomechanical fabrication parameters	* C Ti/C Ti+Al	* C Cr	**	** C	***
PHYSICAL PROPERTIES					
. Thermal Conductivity	*	***		**	
. Thermal Expansion Match with Ferritic Steels (plate, supports)	*	***		**	
MECHANICAL PROPERTIES					
. Elevated temp. tensile	*	**		***	
CORROSION RESISTANCE					
. Resistance to metal loss to stream	**	*		***	
. Resistance to primary side IGSCC	***	*	**	***	
. Resistance to high temp. Phosphate wastage	**	***		**	
. Resistance to Cl^- SCC	*	**	***	***	
. Resitance to OH^- SCC - low conc. 4 g/l - intermediate 100 g/l - high conc. 500 g/l	 *** ** *	 * * **	 ** ** ***	 *** ** **	 *** ***
. Resistance to sulfur compounds pitting	***	**	***	***	

* lower ** intermediate *** higher relative level

Table 4-1: Main alloy characteristics [63].

ii. *Pressurized Heavy Water Reactor:* Monel 400 is a commonly used material or alloy 800.

iii. *Fast reactors* (sodium-sodium heat exchanger): traditional austenitic stainless steels (304, 316, 316L, 316LN), since they require a max temperature of 830K, low primary stresses, and high secondary stresses of thermal origin and excellent heat transfer characteristics of sodium gives rise to thermal fatigue problems/

iv. *Steam generator:* Materials often used are ferritic steels 2.25Cr-lMo, Niobium stabilized 2.25Cr-lMo, 9Cr- IMo and modified 9Cr-lMo (Grade 91), austenitic stainless steel (304/316/321) and Alloy 800. General criteria that need to be fulfilled

are inclusion in pressure vessel codes or availability of adequate data, corrosion resistance under storage(pitting) normal and off-normal chemistry conditions, availability, economics and mechanical properties, such as yield and tensile strength, creep data, low/high cycle fatigue, creep-fatigue interaction, ductility, aging effects, workability, and weldability. Criteria related to use in sodium are mechanical properties in sodium, susceptibility to decarburization, corrosion under normal sodium chemistry conditions, fretting and wear, and corrosion resistance in the case of sodium water reaction (stress corrosion cracking, self-enlargement of leak and impingement wastage). The table below summarizes materials used in steam generators.

Reactor	Status	Superheater(temp.K) Na inlet	Steam outlet	Tubing Material Evaporator	Superheater
Phenix	Operational	823	785	2.25Cr-1Mo 2.25Cr-1Mo+Nb+Ni	SS 321
Superphenix	Operational	798	763	Alloy 800 (once through integrated)	
EFR	Conceptual design completed	798	763	Modified 9Cr-1Mo (91) (once through integrated)	
PFR	Operated for 20 years (Closed)	813	786	2.25Cr-1Mo+Nb+Ni Replacement unit in 2.25Cr-1Mo	SS 316 Replacement tube bundle in 9Cr-1Mo
SNR-300	Built (not operated)	793	773	2.25Cr-1Mo+Nb+Ni	2.25Cr-1Mo+Nb+Ni
EBR-II	Operational	739	711	2.25Cr-1Mo	2.25Cr-1Mo
CRBRP	Designed (not built)	767	755	2.25Cr-1Mo	2.25Cr-1Mo
MONJU	Operational	778	760	2.25Cr-1Mo	SS 321
DFBR	Under design		768	Modified 9Cr-1Mo(91) (once through integrated)	
BN 350	Operational	723	708	2.25Cr-1Mo	2.25Cr-1Mo
BN 600	Operational	793	778	2.25Cr-1Mo	SS 304
BN 800	Under construction	778	763	2.25Cr-1Mo	2.25Cr-1Mo
FBTR	Operational	783	753	2.25Cr-1Mo+Nb+Ni principal material (once through integrated) modified 9Cr-1Mo (91) for future spare modules	
PFBR	Under design	798	763	Modified 9Cr-1Mo(91) (Once through integrated)	

Table 4-2: materials used in steam generators [63].

v. Condensers: Cooling water could contaminate the condensate leading to a variety of corrosion mechanisms. In the table below some materials based on their corrosion resistance are presented. In general, any material that is rated 4 (poor) should be avoided [63].

The next table presents tube materials and their corrosion resistance.

Material	Water Quality	Uniform Corrosion	Pitting & Crevice Running/Stagnant	Inlet End Attack & Erosion-Corrosion	Sulfide Attack	Condensate Grooving Ammoniated and Stress Corrosion Cracking [a]	Impingement Attack [b]
Admiralty Brass	Fresh [c]	2	1/2	2-3	4	4	4
304 & 316 Stainless Steel	Fresh [c,d]	1	2/2	1	1	1	1
Aluminum Brass	Fresh [c] Brackish water Seawater	2	1/3	2-3	4	4	4
90-10-Cu-Ni	Fresh [c] Brackish water Seawater	2	1/2	2	4	2	3
70-30-Cu-Ni [f]	Brackish water Seawater	2	1/2	1-2	4	2	2
Alloy 722	Fresh [c] Brackish water Seawater	2	1/2	1	4	2	2
AL 29-4C [e][f]	Brackish water Seawater	1	1/1	1	1	1	1
Sea-Cure [e][f]	Brackish water Seawater	1	1/1	1	1	1	1
AL-6X [f][g]	Brackish water Seawater	1	1/1	1	1	1	1
Titanium [f]	Brackish water Seawater	1	1/1	1	1	1	1

Note: 1 = excellent, 2 = good, 3 = average, 4 = poor

(a) A rating of 4 eliminates material from being considered acceptable for the air removal section of condenser or from the entire condenser if the tube internal surface deposits will remain on the surface during shutdown.

(b) A rating of 4 eliminates the material from the peripheral zone of the condenser.

(c) Sulfide should not be present for copper alloys; if it is present, note sulfide attack rating column. For 300 series stainless steel, the material should be tested for pitting and crevice corrosion resistance in the actual cooling water if sulfide exceeds 0.1 ppm.

(d) Chloride ion = 70 ppm max for type 304 SS and 300 ppm max for type 316 SS and pH = 5.5-8.0.

(e) Ratings for 29-4C and Sea Cure are based on experimental data. There is relatively little operating experience with these alloys and the selection decision should include a review of the experience to date.

(f) These tube materials are suitable for fresh water, but are seldom cost effective for fresh water.

(g) The pitting and crevice rating given is tentative and may change based on the findings of tube failure analyses that were not completed at the printing of this report.

Table 4-3: tube materials and their corrosion resistance [63].

4.1.2 Thermal design and sizing

Heat exchangers' sizing is important considering their effectiveness, and initial and operational cost. A practical method is the P_1-P_2 method [65].

4.1.3 Inspection recommendations

Considering the inspection of heat exchangers some basic screening techniques that have been given include the following. Regarding ferrous tubes, the use of magnetic flux leakage in case of limited pitting corrosion and the use of remote field eddy current testing in case of extended pitting corrosion and wall thickening. Regarding non-ferrous tubes eddy current testing is proposed in case of pitting corrosion, wall thickening, and cracks. Finally, an internal rotary inspection system can be used to verify magnetic flux leakage, remote field eddy current testing, and eddy current testing. The last one can only be used in tubes where the above techniques have been identified [56].

4.2 Preventing Common Issues

4.2.1 Steam and water hammer

Countermeasures of this failure mode require the use of elbows in U-tubes, the use of flow restricting orifice in the inlet of the tube, and the use of a steam trap to remove the condensate as well as condensate pumps. The software can be used to estimate parameters such as slug formation, steam bubble condensation, peak pressure, and pressure surge. Finally, raising the temperature in the inlet while reducing the flow rate and maintaining a superheated stream with limited glow velocity will help protect the susceptible regions [11].

4.2.2 Vibrational failures

This mode of failure can be avoided by using materials with a high modulus of elasticity and increasing the tolerance of the wall thickness. Anti-vibration bars or spacers are also suggested. The manufacturer needs to provide coatings and proper clearance. The shedding and the acoustic frequency must be controlled [11]. Regarding frequency, an application of flow-stimulated vibration assessment can be used during the early stages to increase the natural frequency or reduce the forcing frequency. Finally, baffle support or strip baffles at the U-bend need to be provided [17].

4.2.3 Creep rupture

To avoid the results of creep rupture some preventive procedures that can be followed include the use of better heat-resisting materials, the inspection of the metals that have been used, and specifically the base and weld metals. Cleaning and controlling fluid chemistry have to be a part of routine maintenance to avoid the formation of deposits in the inner and outer surfaces of the tubes [18].

4.2.4 Hydrogen attack

The root cause of failure is induced by the presence of hydrogen (H_2) in temperatures above 205^{o}C. In this case, residual stresses or high applied loads can minimize the catastrophic results that might occur [18].

4.2.5 Thermal fatigue

Thermal fatigue or thermal fatigue cracking as a result of poor water circulation rising thermal cycling or thermal cycling, in general, can be treated by maintaining proper operating conditions and/or controlling the formation of corrosion products to optimize the heat exchanger operation [18]. The inspection of the temperature in short periods is suggested with the use of control devices. The identification of sites prone to thermal cycling will speed up the recognition process of the failure mode as well as routine quality inspections [11].

4.2.6 Freeze-up

To avoid the temperature, falling below the freezing point air flow control of louvers can be adjusted in the air-cooled heat exchanger. Rolling-type windbreakers, partial through-flow tower shells, and alternation of windbreaker configurations can be used. Finally, regular adjustments of the air and the water flow rate at intervals will reduce failure risks due to freeze-up [11].

4.2.7 Corrosion protection

Pitting corrosion

Since the presence of specific elements such as vanadium, chlorine, etc. reinforces pitting corrosion the addition of chromium, zirconium, and molybdenum is suggested, while at the same time, the reduction of chloride below 50 ppm is encouraged. Structural issues like joints need to be frequently checked regarding the temperature. As far as welding is concerned nitrogen as shielding gas with argon in the gas metal arc is suggested. Another measure to enhance pitting resistance is to conduct reverse osmosis for the fed water [11], which can be achieved by controlling the desalination process until the desired level [26]. The chloride ions and water vapor are other aspects that need to be checked in small periods [11]. to increase the chlorides in the water the use of hydrochloric acid (HCl) is prohibited but sulfuric acid can be safely used [26].

Stress corrosion cracking

The following figure presents a percentage of materials in SCC cases.

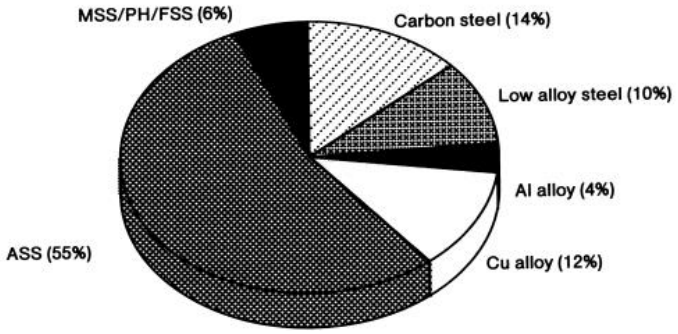

Figure 4-1: Percentage of materials in SCC cases [41].

Correcting measures can be summarized in the following table [41].

environment	material change	heat treatment	SR	structural change	machining operation	welding	covering	environment	operating condition	cleaning inspection	unavoidable	case numbers
mild steel												
air	1	2	1	1	1							14
miscellaneous*	2	1	5	1	1	1	1	1	1	1		11
sum	3	3	6	2	2	1	1	1	1	1		15/21
*sea water, oil, NH_3 chemical												
low alloy steel												
H_2S	4	2	1		1	1					1	7
natural environment	2	2		3	1			1	1			4
sum	6	4	1	3	2	1		1	1		1	11/20
Al alloy												
ocean	2			1			3			3		3
air	1											1
sum	3			1			3			3		4/10
Cu alloy												
water	6		1	1	2				2	1		8
sea water	2			1	1							2
NH_3, Hg	3	1	1									3
sum	11	1	2	2	3				2	1		13/22
ASS												
heat insulator, filling material							3	4				5
water	4		3	2	3	2		2	3	2		11
air	3		1	1	1	1	2					6
steam	4		2	2	1			2				9
alkaline	4	1	2	1	1	1		1	2	5		6
chemical plant	9	1	2	1	1	1	1	1				11
oil	8	3		1	2					5		12
sum	32	5	10	8	9	5	6	10	5	8		60/98
*H_2S + CO_2, hot air, seacoast												
MSS,PH,FSS												
water		4			1							4
miscellaneous*	3	1			2		1					3
sum	3	5			3		1					7/12
H_2S + CO_2, hot air, seacoast												

Table 4-4: Summarized correcting methods

Finally, in the following figure, the percentage of correcting measures is presented [41].

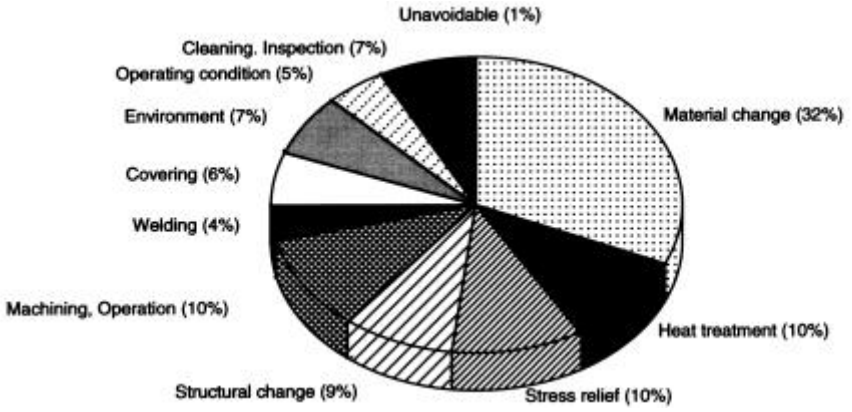

Figure 4-2: percentage of correcting measures in SCC cases [41].

Based on the above figure it is obvious that most cases demand material change (32%) and a few heat treatment (10%) and stress relief (10%) [41].

The effects of the presence of chlorides in combination with high residual stresses can be treated by annealing. Tubes that have been annealed are less likely to present residual stresses [8].

Galvanic corrosion

As preventive measures for galvanic corrosion proper design, proper material selection, and effective maintenance are most often suggested [17].

Crevice corrosion

To avoid the results of crevice corrosion all kinds of crevices need to be evaded in structural design and complete weld penetration has to be ensured. Periodic cleaning and proper material selection will also minimize the probability of this mode of failure appearing [17].

Corrosion fatigue

The following figure presents a percentage of correcting measures in CF cases.

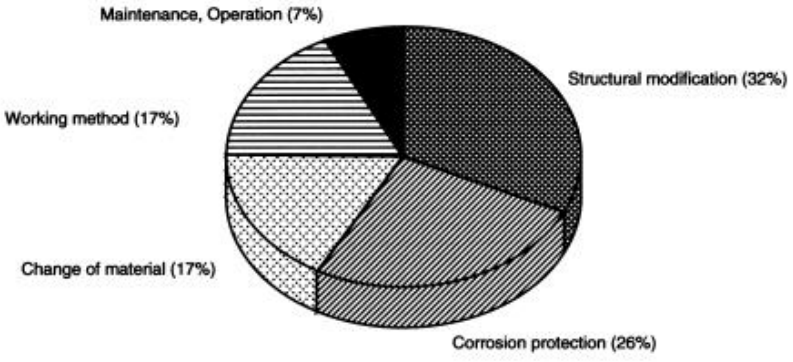

Figure 4-3: Percentage of correcting measures in CF cases [41].

Noticing that structural modification is the most important corrective measure, stress analysis is mandatory in the presence of a corrosion fatigue environment [41].

A common solution to corrosion fatigue is the use of admiralty brass due to their good corrosion resistance. Annealing after mending is suggested to reduce residual stresses [8]. Another material recommendation is the use of Al-brass or cupro-nickel alloys [18]. In addition, some more countermeasures against corrosion fatigue are the provision of protective coating, cathodic protection, and the addition of inhibitors. Finally, compressive stresses can be induced by shot peening [11].

Erosion-Corrosion

Erosion-corrosion as a result of turbulent and disturbed water with solid particles can be avoided by reducing the velocity of the water and by using the right water filters. Infiltration techniques and magnetic particles can be proven quite useful. This will minimize the solid particles and the protective layer will not be destabilized by the chemical composition of the water [11,39].

In case this type of corrosion is repetitive inside the elbow to lessen its influence on the flow field at the elbow, a smaller thermocouple can be used, or the thermocouple can be moved further away from the elbow. Additionally, to minimize the impact of fluid, an elbow with a higher curvature radius can be used. Finally, pipe fittings lined with polytetrafluoroethylene (PTFE) can also be used to prevent corrosive media from coming into contact with the pipe [40].

Other measures to be taken into consideration are the use of resistant material, the use of prismatic flow correcting devices, and the provision of protective coatings like ceramic coatings carbide, and nitride coatings. In addition, the shape, the geometry, and the design of parts inside or outside the tube need to be improved according to the given specifications. Finally, cathodic protection, control of the PH of the fluid, and reduction of oxygen are some basic countermeasures [11].

Fouling

Fouling is an important mode of failure mainly induced by undesired particles and salts, reinforced by the low velocity at the entrance, low wall temperature, and high concentration of elements like molybdenum, oxygen, chlorine, and vanadium. To address this issue, there are many suggestions from the scientific community. Double perforated impingement plates can be used to regulate the flow and reduce the accumulation. Gum Arabic can also be used

as a stabilizer to create a smooth solution. Regarding cleaning, an easy design will facilitate the process which may include an alkaline or acidic wash cycle and inline gas rumbling. Chemical cleaning is a choice but in case mechanical means are chosen, inserts, scrappers, projectiles and wire brushes can be used. Other cleaning processes include moving rubber balls and scraping, water blast cleaning, cleaning using brushes, jetting pressurized air, and back flushing. Finally, regarding cleaning ice or nitrogen purging, desalting and caustic scrubbing can be performed. In addition, surface preparations and epoxy coating on the surface of the tube can help minimize the effects of fouling [11].

4.2.9 Structural integrity and mechanical design

According to the existing literature, two rid designs are proposed, air-to-air rig design and oil-to-air rig design.

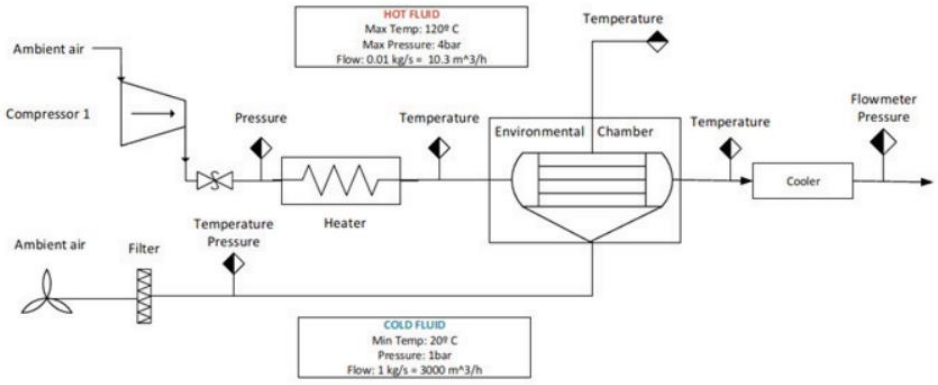

Figure 4-4: Air-to-air rig design [12].

As can be seen in the above figure air-to-air consists of a cold and a hot open circuit. The hot end of the rig begins with compressed air from the compressor. Following that, a heater boosts the temperature of the air, which can be monitored by the temperature sensor before passing through the heat exchanger. Temperature is measured again at the heat exchanger's outlet to monitor its performance. A cooler will chill the exhaust before it is exhausted, reducing it to tolerable levels. A blower pushes ambient air through the filter to the heat exchanger, which is subsequently exhausted.

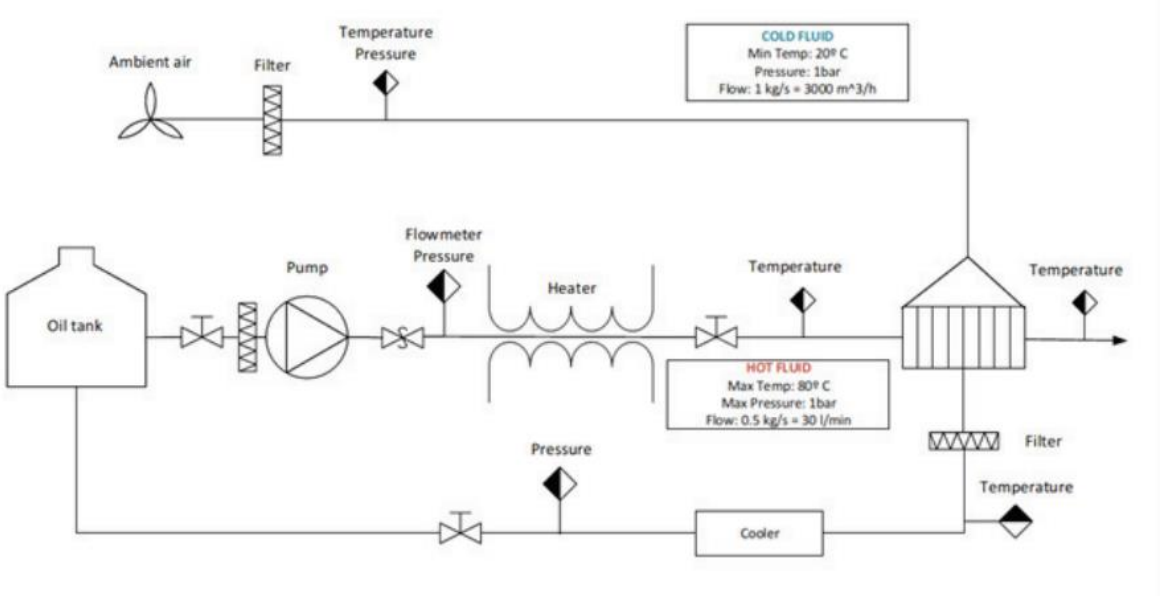

Figure 4-5: Oil-to-air rig design [12].

The oil-to-air heat exchanger rig is made up of a hot circuit (closed loop system) and a cold circuit (open system). The hot one starts with an oil tank to store the fluid, followed by a pump that pulls it from the container and pushes it through a filter into the system. The oil is then passed through the heater and its temperature is recorded before entering the heat exchanger. The temperature of the oil as it exits the heat exchanger is also measured before it is cooled and returned to the oil tank. The cold air circuit stays unchanged from the air-to-air rig design [12].

4.3 Manufacturing Routes and machine learning

The tube's end and specifically the joint zone tends to appear residual stress usually as a result of the rolling-in joining technique. This creates residual stresses that lead to a variety of corrosion-based failures. Recommendations given to manufacturers include avoiding excessive wall reduction and tube extrusion to decrease the residual stress at the end of the tubes (tube-to-tube sheet joints). Another measure is heat treatment or shot peening after rolling the tube ends to the tube sheet [44].

Failure can also be predicted with the use of machine learning. Many algorithms have been developed such as Support Vector Machines (SVM), Deep Neural networks (DNNs), Cluster analysis, etc. In 2020 a powerful deep neural network model was created by Sreenath Sundar to predict fouling in heat exchangers. This network mainly uses historical operation data. There have also been investigated six alternative machine learning techniques by Aláiz-Moretón et al: adaptive boosting, gradient boosting, random decision forests, an external neural network for detection fault detection of a Geothermal Heat Exchanger, highly

randomized trees, and k-nearest neighbors. Although many algorithms have been developed only a few of them have been tested in real-life situations [17].

4.4 Maintenance and Cleaning Programs

4.4.1 Maintenance

Maintenance is categorized into preventive and predictive. The first one involves the operation of the heat exchanger until its failure. Since the equipment is working until a possible shutdown, the replacement or repair of the failed part will probably require a lot of time making the method ineffective and expensive.

Predictive maintenance can be achieved based on the historical operating data of the heat exchanger. Advanced analytics can be used to predict possible failures. Hence, maintenance cost is reduced, productivity increases and breakdowns are limited or even zeroed out. Another advantage of predictive maintenance is that no secondary damages appear since the failure is dealt with before it even occurs. The main aspects that predictive maintenance focuses on are downtime saving, cost saving, health of equipment, noisy dataset, and lifespan of equipment [17].

Software tools are often used to enhance the reliability of the heat exchanger components and optimize their efficiency. Many issues such as the type of welding, the impact of manufacturing costs, the robustness, the increment of maximum mechanical resistance, or the reduction of lost opportunity costs are related to heat exchanger shutdowns or operating problems. At the same time, fouling seems to appear as a significant parameter to maintenance issues. Concerning the above the use of software tools will help achieve a 30% decrease in annual maintenance costs. This software analyzes not only the causes of failure but also uses prediction models based on probabilities related to cleaning, investigates the roots of failure, and calculates the maintainability and reliability of the components [64]. Concerning fouling great efforts have been made to develop preventive maintenance scheduling tools, since it affects both the reliability and the workability of the heat exchanger. Neural network models have been developed using statistical and historical operating data [66].

4.4.2 Cleaning

In general cleaning PIGS and hydro drilling techniques are usually used, while this application of optimal pressurized cleaning medium is suggested. The medium has to be filtered for better results and there is a general preference for chemical cleaning over

mechanical cleaning [11]. Two types of cleaning are usually used to maintain and/or restore heat exchangers' efficiency or even maintain performance without interrupting the process, online and offline cleaning. The choice of which method is to be used depends on the characteristics of each case. The first one uses mechanical methods on the tube side and although it provides continuity, is high-priced and does not guarantee complete cleaning. Some methods are the circulation of sponge rubber balls, two phases of the ferrous sulfate treatment, chlorination used for combat bio-fouling, scale inhibitors, magnetic devices, sonic technology, injection of chemical solutions, and the use of radiation. Offline cleaning requires the process to stop. There are two categories, chemical and mechanical cleaning. Access to inside surfaces is needed and the following methods exist, tube drilling and rodding, and cleaning with explosives [67].

5. CONCLUSIONS

To conclude, this paper has delved into the most common failure mechanisms in heat exchangers accompanied by root causes and guidelines leveraging a series of case studies assigned to the Laboratory of Materials, University of Thessaly. Through these case studies and studying the theoretical background regarding the operation of a heat exchanger an empirical guide can be provided. This paper has unveiled a multifaceted approach, underlining that the failure mechanisms of heat exchangers appear to be an intricate combination of many factors. Since a reliable and efficient operation of these important components is not just a technical endeavor but also an important aspect for many industries, their right and safe operation needs to be precise.

Through a careful analysis of the existing bibliography, the main modes of failure can be summarized in four main categories, mechanical, chemically induced corrosion, a combination of mechanical and chemically induced corrosion, and fouling. The first one involves erosion, steam, and water hammer, vibrational failures, thermal fatigue, freeze-up, loss of cooling water, and thermal expansion. The second one involves general corrosion, dealloying, pitting corrosion, stress corrosion cracking, galvanic corrosion, crevice corrosion, and condensate grooving. As a result of a combination of the two previous categories, erosion-corrosion and corrosion-fatigue appear to exist. Finally, fouling involves precipitate fouling- scaling, corrosion-based fouling, and biofouling.

Investigating the root causes that lead to the modes of failure that have been mentioned above we come across structural, operational, metallurgical causes and design issues. The first ones involve welding and manufacturing defects as well as inadequate support and alignment. Operational root causes concern working parameters, elevated temperatures, and the existing environment. Finally, metallurgy is related to phase transformation, while design issues are a separate category.

To identify and analyze the above failure mechanisms in heat exchangers there have been developed many types of inspection. The following are a few of the well-known heat exchanger inspection methods: Laser Inspection, Ultrasonic Testing (UT), Internal Rotary Inspection System (IRIS), Remote Field Testing (RFT), Remote-Field Array (RFA), Near-Field Array (NFA), Radiographic Testing (RT), Eddy Current Testing (ECT), Acoustic Emission Testing (AET), Near-Field Testing (NFT), Infrared Thermography (IRT), Magnetic Flux Leakage (MFL), Tangential Eddy Current Array (TECA), Eddy Current Array (ECA), Transverse Field Inspection (TFI) and Partial Saturation Eddy Currents (PSEC). Some of the above methods are briefly presented in a previous chapter.

As the theoretical background of this paper is concluded it is paramount to acknowledge and assess the impacts of heat exchanger failures, as they raise economic, safety, and environmental concerns.

As an ultimate goal, this paper provides a comprehensive guideline set pointing out that by attaining these objectives improvement in the reliability, performance, and operational efficiency of heat exchangers can be achieved through the creation of practices that will minimize failure modes. The main takeaways from the presented guidelines are summarized in the following categories, design considerations, the prevention of common issues, manufacturing routes and machine learning as well as maintenance and cleaning programs.

These guidelines, rooted in deep research by a large part of the scientific community as a result of previous failures and theoretical approaches are not just a collection of recommendations but also a commitment to the future of heat exchangers. By adopting these guidelines, industries not only ensure a safer, more efficient, and more reliable process but also embrace a future committed to progress and innovation.

REFERENCES

[1] https://www.bendel.com/

[2] Gao, W., Li, J., Li, Y., & Kong, L. (2020). Numerical identification of critical erosion-prone areas in tube heat exchangers. *Engineering Applications of Computational Fluid Mechanics*, *14*(1), 1429–1444. https://doi.org/10.1080/19942060.2020.1835735

[3] Baskar, P. (2019b). Four Types of Heat Exchanger Failures . . . mechanical, chemically induced corrosion, a combination of mechanical and chemically induced corrosion, and scale, mud, and algae fouling. *www.academia.edu*. https://www.academia.edu/40217020/Four_Types_of_Heat_Exchanger_Failures_mechanical_chemically_induced_corrosion_combination_of_mechanical_and_chemically_induced_corrosion_and_scale_mud_and_algae_fouling

[4] Ranjbar, K. (2010). Effect of flow-induced corrosion and erosion on failure of a tubular heat exchanger. *Materials in Engineering*, 31(1), 613–619. https://doi.org/10.1016/j.matdes.2009.06.025

[5] Badr, H. M., Habib, M. A., Ben-Mansour, R., Said, S., & Al-Anizi, S. S. (2006). Erosion in the tube entrance region of an air-cooled heat exchanger. *International Journal of Impact Engineering*, *32*(9), 1440–1463. https://doi.org/10.1016/j.ijimpeng.2005.01.008

[6] Sun, Q., Tang, S., Wang, F. L., & Zhao, Q. (2017). Gas-side fouling, erosion and corrosion of heat exchangers for middle/low-temperature waste heat utilization: A review on simulation and experiment. *Applied Thermal Engineering*, *126*, 737–761. https://doi.org/10.1016/j.applthermaleng.2017.07.095

[7] Wojnar, W. (2013). Erosion of heat exchangers due to soot blowing. *Engineering Failure Analysis*, *33*, 473–489. https://doi.org/10.1016/j.engfailanal.2013.06.026

[8] Powell, G. W., & Mahmoud, S. E. (1986). *ASM Metals Handbook* (Vol. 11).

[9] Pelliccione, A., Silva, L., Silva, F., & Silva, O. (2019). Dealuminification of heat exchanger tubes. *Engineering Failure Analysis*, *105*, 970–981. https://doi.org/10.1016/j.engfailanal.2019.07.052

[10] Streicher, W. (2001). Minimising the risk of water hammer and other problems at the beginning of stagnation of solar thermal plants — a theoretical approach. *Solar Energy*, *69*, 187–196. https://doi.org/10.1016/s0038-092x(01)00018-4

[11] Thekkuden, D. T., Mourad, A. I., & Bouzid, A. (2021). Failures and leak inspection techniques of tube-to-tubesheet joints: A review. *Engineering Failure Analysis*, *130*, 105798. https://doi.org/10.1016/j.engfailanal.2021.105798

[12] Addepalli, S., Eiroa, D., Lieotrakool, S., François, A., Guisset, J., Sanjaime, D., Kazarian, M., Duda, J., Roy, R., & Phillips, P. S. (2015). Degradation study of heat exchangers. *Procedia CIRP*, *38*, 137–142. https://doi.org/10.1016/j.procir.2015.07.057

[13] Weaver, D., & Fitzpatrick, J. (1988). A review of cross-flow induced vibrations in heat exchanger tube arrays. *Journal of Fluids and Structures*, *2*(1), 73–93. https://doi.org/10.1016/s0889-9746(88)90137-5

[14] Goyder, H. (2002). Flow-Induced vibration in heat exchangers. *Chemical Engineering Research & Design*, *80*(3), 226–232. https://doi.org/10.1205/026387602753581971

[15] Pettigrew, M. J., & Taylor, C. E. (2003b). Vibration analysis of shell-and-tube heat exchangers: an overview—Part 2: vibration response, fretting-wear, guidelines.

Journal of Fluids and Structures, *18*(5), 485–500. https://doi.org/10.1016/j.jfluidstructs.2003.08.008

[16] Hoseinzadeh, S., & Heyns, P. (2020). Thermo-structural fatigue and lifetime analysis of a heat exchanger as a feedwater heater in power plant. *Engineering Failure Analysis*, *113*, 104548. https://doi.org/10.1016/j.engfailanal.2020.104548

[17] Ezuber, H. M., & Hossain, S. M. Z. (2022). A review of corrosion failures in shell and tube heat exchangers: roots and advanced counteractive. *Heat and Mass Transfer*, *59*(6), 971–987. https://doi.org/10.1007/s00231-022-03301-3.

[18] Ali, M., Ul-Hamid, A., Alhems, L. M., & Saeed, A. (2020). Review of common failures in heat exchangers – Part I: Mechanical and elevated temperature failures. *Engineering Failure Analysis*, *109*, 104396. https://doi.org/10.1016/j.engfailanal.2020.104396

[19] Erol, S., & Baudin, F. (2016). Freeze damage of grouting materials for borehole heat exchanger: Experimental and analytical evaluations. *Geomechanics for Energy and the Environment*, *5*, 29–41. https://doi.org/10.1016/j.gete.2015.12.002

[20] Ratna, D. (2012). Thermal properties of thermosets. In *Elsevier eBooks* (pp. 62–91). https://doi.org/10.1533/9780857097637.1.62

[21] Brown, W., & Reeves, D. (2000). Failure of heat exchanger gaskets due to differential radial expansion of the mating flanges. *ResearchGate*. https://www.researchgate.net/publication/293545804_Failure_of_heat_exchanger_gaskets_due_to_differential_radial_expansion_of_the_mating_flanges

[22] Janikowski, D. S. (2007). Selecting tubing materials for power generation heat exchangers. *ResearchGate*. https://www.researchgate.net/publication/237336864_Selecting_Tubing_Materials_for_Power_Generation_Heat_Exchangers

[23] *Shreir's corrosion*. (n.d.). ScienceDirect. https://www.sciencedirect.com/referencework/9780444527875/shreirs-corrosion

[24] https://www.ddcoatings.co.uk/2276/what-is-pitting-corrosion

[25] Liu, D., Hu, J., Yuan, X., Zhou, L., & Zhong, X. (2022). Failure analysis and experimental verification on the hydrogen-driven pitting corrosion of heat exchanger tube material. *Engineering Failure Analysis*, *137*, 106283. https://doi.org/10.1016/j.engfailanal.2022.106283

[26] Ghayad, I. M., Hamid, Z. A., & Gomaa, N. (2015). A case study: Corrosion failure of tube heat exchanger. *Journal of Metallurgical Engineering*, *4*(0), 57. https://doi.org/10.14355/me.2015.04.007

[27] Khodamorad, S., Alinezhad, N., Haghshenas, D. F., & Ghahtan, K. (2016). Stress corrosion cracking in Type.316 plates of a heat exchanger. *Case Studies in Engineering Failure Analysis*, *5–6*, 59–66. https://doi.org/10.1016/j.csefa.2016.03.001

[28] Pola, A., Gelfi, M., Depero, L. E., & Roberti, R. (2008). Study of annealing temperature effect on stress-corrosion cracking of aluminum brass heat-exchangers tubes by microdiffraction experiments. *Engineering Failure Analysis*, *15*(1–2), 54–61. https://doi.org/10.1016/j.engfailanal.2007.01.004

[29] Xu, S., Wang, C., & Wang, W. (2015). Failure analysis of stress corrosion cracking in heat exchanger tubes during start-up operation. *Engineering Failure Analysis*, *51*, 1–8. https://doi.org/10.1016/j.engfailanal.2015.02.005

[30] Tawancy, H. (2009). Failure of hydrocracker heat exchanger tubes in an oil refinery by polythionic acid-stress corrosion cracking. *Engineering Failure Analysis*, *16*(7), 2091–2097. https://doi.org/10.1016/j.engfailanal.2009.02.002
[31] Subramanian, C., Ghosh, D., Reddy, D., Ghosh, D., Natarajan, R., & Velavan, S. (2022). Stress corrosion cracking of U tube heat exchanger used for low pressure steam generation in a hydrogen unit of petroleum refinery. *Engineering Failure Analysis*, *137*, 106245. https://doi.org/10.1016/j.engfailanal.2022.106245
[32] Cho, S., Kim, S., Kim, W., & Kim, J. (2019). Stress corrosion cracking of heat exchanger tubes in district heating system. *Corrosion Science and Technology*, *18*(2), 49–54. https://doi.org/10.14773/cst.2019.18.2.49
[33] Lachowicz, M., Lachowicz, M., & Gertruda, A. (2022). Assessment of the possibility of galvanic corrosion in aluminum microchannel heat exchangers. *Crystals*, *12*(10), 1439. https://doi.org/10.3390/cryst12101439
[34] https://captaincorrosion.com/crevice-corrosion/
[35] Panahi, H., Eslami, A., Golozar, M., & Laleh, A. A. (2020). An investigation on corrosion failure of a shell-and-tube heat exchanger in a natural gas treating plant. *Engineering Failure Analysis*, *118*, 104918. https://doi.org/10.1016/j.engfailanal.2020.104918
[36] Fan, Z., Du, J., Zhang, Z., Ma, Y., Cao, S., Niu, K., & Liu, C. (2019). Internal leakage of plate heat exchangers caused by cooperation of pitting, crevice corrosion, and fretting. *Engineering Failure Analysis*, *96*, 340–347. https://doi.org/10.1016/j.engfailanal.2018.10.007
[37] Ranjbar, K., & Sharifi, E. (2023). Failure assessment of heat exchanger tubes due to grooving corrosion. *Journal of Failure Analysis and Prevention*, *23*(2), 739–750. https://doi.org/10.1007/s11668-023-01589-9
[38] Cheng, Y. F. (2011). Erosion-accelerated corrosion in flow systems: the behavior of aluminum alloys in automotive cooling systems. In *Elsevier eBooks* (pp. 475–500e). https://doi.org/10.1533/9780857093738.3.475
[39] Kuźnicka, B. (2009). Erosion–corrosion of heat exchanger tubes. *Engineering Failure Analysis*, *16*(7), 2382–2387. https://doi.org/10.1016/j.engfailanal.2009.03.026
[40] Yan, Z., Wang, L., Zhang, P., Sun, W., Yang, Z., Bingyan, L., Tian, J., Shu, X., He, Y., & Liu, G. (2021). Failure analysis of Erosion-Corrosion of the bend pipe at sewage stripping units. *Engineering Failure Analysis*, *129*, 105675. https://doi.org/10.1016/j.engfailanal.2021.105675
[41] Komai, K. (1998). Failure analysis and prevention in SCC and corrosion fatigue cases. *International Journal of Fatigue*, *20*(2), 145–154. https://doi.org/10.1016/s0142-1123(97)00098-4
[42] Ravindranath, K., Tanoli, N., & Gopal, H. (2012b). Failure investigation of brass heat exchanger tube. *Engineering Failure Analysis*, *26*, 332–336. https://doi.org/10.1016/j.engfailanal.2012.07.018
[43] De Farias Azevedo, C. R., & Alves, G. S. (2005). Failure analysis of a heat-exchanger serpentine. *Engineering Failure Analysis*, *12*(2), 193–200. https://doi.org/10.1016/j.engfailanal.2004.07.001
[44] Zahrani, E. M. (2020). Premature failure of Grade-316TI stainless steel tubing in a boiler Feed-Water heat exchanger in a steel complex. *Journal of Failure Analysis and Prevention*, *21*(1), 61–73. https://doi.org/10.1007/s11668-020-01037-y
[45] https://www.youtube.com/watch?v=sTYIw-w-fJo&ab_channel=SkillLync

[46] Ranjbar, K. (2010d). Effect of flow induced corrosion and erosion on failure of a tubular heat exchanger. *Materials in Engineering*, *31*(1), 613–619. https://doi.org/10.1016/j.matdes.2009.06.025
[47] Besghaier, R., Dhouibi, L., Chaouachi, B., & Jeannin, M. (2021). Heat exchanger failure analysis in the simulated marine environment: Prediction of the fouling removal temperature. *Engineering Failure Analysis*, *122*, 105243. https://doi.org/10.1016/j.engfailanal.2021.105243
[48] Vasauskas, V., & Baskutis, S. (2006). Failures and fouling analysis in heat exchangers. *ResearchGate*. https://www.researchgate.net/publication/237276069_Failures_and_fouling_analysis_in_heat_exchangers
[49] Sun, Q., Tang, S., Wang, F. L., & Zhao, Q. (2017b). Gas-side fouling, erosion and corrosion of heat exchangers for middle/low temperature waste heat utilization: A review on simulation and experiment. *Applied Thermal Engineering*, *126*, 737–761. https://doi.org/10.1016/j.applthermaleng.2017.07.095
[50] *StackPath*. (n.d.). https://www.watertechonline.com/process-water/article/14071807/understanding-and-preventing-heat-exchanger-fouling
[51] Obrutsky, L. (n.d.). *Eddy current technology for heat exchanger and steam generator tube inspection*. https://inis.iaea.org/search/search.aspx?orig_q=RN:37043871
[52] https://americanefficiency.com/eddy-current-testing/
[53] *Internal Rotary Inspection System (IRIS) | EddyFi*. (n.d.). https://www.eddyfi.com/en/technology/internal-rotary-inspection-system-iris
[54] Saffiudeen, M. F., Syed, A., & Mohammed, F. T. (2021). Failure analysis of heat exchanger using Internal Rotary Inspection System (IRIS). *Journal of Failure Analysis and Prevention*, *21*(2), 494–498. https://doi.org/10.1007/s11668-020-01093-4
[55] https://industrial.evidentscientific.com.cn/en/insight/a-faster-way-to-inspect-heat-exchanger-tubes/
[56] Al-Qadeeb, F. E. (2005). „Tubing inspection using multiple NDT techniques". *ResearchGate*. https://www.researchgate.net/publication/229009890_Tubing_inspection_using_multiple_NDT_techniques
[57] Sadek, H. (2006). NDE technologies for the examination of heat exchangers and boiler tubes – principles, advantages and limitations. *Insight*, *48*(3), 181–184. https://doi.org/10.1784/insi.2006.48.3.181
[58] https://www.explosionproofvideoscopes.com/heat-exchanger-inspection/
[59] Corleto, C. R., & Argade, G. (2017). Failure analysis of dissimilar weld in heat exchanger. *Case Studies in Engineering Failure Analysis*, *9*, 27–34. https://doi.org/10.1016/j.csefa.2017.05.003
[60] Otegui, J., & Fazzini, P. (2004). Failure analysis of tube–tubesheet welds in cracked gas heat exchangers. *Engineering Failure Analysis*, *11*(6), 903–913. https://doi.org/10.1016/j.engfailanal.2004.01.003
[61] Solomon, N., & Solomon, I. J. (2017). Effect of deformation-induced phase transformation on AISI 316 stainless steel corrosion resistance. *Engineering Failure Analysis*, *79*, 865–875. https://doi.org/10.1016/j.engfailanal.2017.05.031
[62] Reitz, W. (2002). SO2 heat exchanger failure. *Practical Failure Analysis*. https://doi.org/10.1007/bf02719189
[63] Rodriguez, P. (1997). Selection of materials for heat exchangers. Web.

[64] Sikos, L., & Klemeš, J. J. (2010). Reliability, availability, and maintenance optimisation of heat exchanger networks. *Applied Thermal Engineering*, *30*(1), 63–69. https://doi.org/10.1016/j.applthermaleng.2009.02.013

[65] Söylemez, M. S. (2000). On the optimum heat exchanger sizing for heat recovery. *Energy Conversion and Management*, *41*(13), 1419–1427. https://doi.org/10.1016/s0196-8904(99)00181-8

[66] Radhakrishnan, V., Ramasamy, M., Zabiri, H., Thanh, V., Tahir, N., Mukhtar, H., Hamdi, M., & Ramli, N. M. (2007). Heat exchanger fouling model and preventive maintenance scheduling tool. *Applied Thermal Engineering*, *27*(17–18), 2791–2802. https://doi.org/10.1016/j.applthermaleng.2007.02.009

[67] Murshed, S. M. S., & Lopes, M. (2017). *Heat Exchangers - Advanced features and applications*. https://doi.org/10.5772/68064